Science of Remote Sensing 8 (2023) 100107

Contents lists available at ScienceDirect

Science of Remote Sensing

journal homepage: www.sciencedirect.com/journal/science-of-remote-sensing

Mapping subcanopy light regimes in temperate mountain forests from Airborne Laser Scanning, Sentinel-1 and Sentinel-2

Felix Glasmann [a,*], Cornelius Senf [b], Rupert Seidl [b,c], Peter Annighöfer [a]

[a] Technical University of Munich, School of Life Sciences, Forest and Agroforest Systems, Hans-Carl-v.-Carlowitz-Platz 2, 85354, Freising, Germany
[b] Technical University of Munich, School of Life Sciences, Ecosystem Dynamics and Forest Management Group, Hans-Carl-v.-Carlowitz-Platz 2, 85354, Freising, Germany
[c] Berchtesgaden National Park, Doktorberg 6, 83471, Berchtesgaden, Germany

ARTICLE INFO

Keywords:
Airborne Laser Scanning
Sentinel-1
Sentinel-2
Light regime
Forest structure

ABSTRACT

Sunlight is the primary source of energy in forest ecosystems and subcanopy light regimes largely determine the establishment, growth and dispersal of plants and thus forest floor plant communities. Subcanopy light regimes are highly variable in both space and time, which makes monitoring them challenging. In this study, we assess the potential of Sentinel-1 and Sentinel-2 time series for predicting subcanopy light regimes in temperate mountain forests. We trained different random forest regression models predicting field-measured total site factor (TSF, proportion of potential direct and diffuse solar radiation reaching the forest floor, here defined as the transition zone between belowground and aboveground biomass) from a set of metrics derived from Sentinel-1 and Sentinel-2 time series. Model performance was benchmarked against a model based on structural metrics derived from Airborne Laser Scanning (ALS) data, serving as an empirical gold-standard in modelling subcanopy light regimes. We found that Sentinel-1 and Sentinel-2 time series performed nearly as good as the model based on high-resolution ALS data (R^2/RMSE of 0.80/0.11 for Sentinel-1/2 compared to R^2/RMSE of 0.90/0.08 for ALS). We furthermore tested the generalizability of the trained models to two new sites not used for training for which field data was available for validation. Prediction accuracy for the ALS model decreased substantially for the two independent test sites due to variable ALS data quality and acquisition date (ΔR^2/ΔRMSE of 0.29/0.05 and 0.11/0.03 for both independent test sites). The prediction accuracy of the Sentinel-1/2 model, however, remained more stable (ΔR^2/ΔRMSE of 0.13/0.02 and 0.13/0.04). We therefore conclude that a combination of Sentinel-1 and Sentinel-2 time series has the potential to map subcanopy light conditions spatially and temporally independent of the availability of high-resolution ALS data. This has important implications for the operational monitoring of forest ecosystems across large scales, which is often limited by the challenges related to acquiring airborne datasets.

1. Introduction

Forest ecosystems cover about 31% of the earth's surface and provide important ecosystem services to humanity (FAO, 2022). These ecosystem services include climate regulation and carbon sequestration, watershed protection, the production of timber, as well as various other non-timber forest products (Forest Europe, 2020). To safeguard the provision of these manifold ecosystem services for future generations, it is of utmost importance to understand and monitor the key components and dynamics of forest ecosystems and their interactions with the biotic and abiotic environment. One central characteristic of forest ecosystems is that they modulate the subcanopy light availability. Light is the source of energy for photosynthetic activity of autotrophic organisms and – together with water, nutrients and appropriate thermal conditions – one of the four basic requirements for plant growth (Kimmins, 2004; Nemani et al., 2003; Oliver and Larson, 1996). Light also largely determines forest microclimate (Hardwick et al., 2015; Heithecker and Halpern, 2006; Ritter et al., 2005; Schmidt et al., 2017; Thom et al., 2020), which is closely related to the water cycle (Giuggiola et al., 2016), biodiversity (Dormann et al., 2020; Lettenmaier et al., 2022), as well as local decomposition processes and nutrient cycles (Seibold et al., 2016, 2021). Furthermore, the availability of light is a strong determinant of the establishment and growth of trees in the regeneration layer (Su et al., 2019). For that reason, the local light regime can be a decisive factor in

* Corresponding author.
E-mail address: felix.glasmann@tum.de (F. Glasmann).

https://doi.org/10.1016/j.srs.2023.100107
Received 18 September 2023; Received in revised form 30 October 2023; Accepted 4 November 2023
Available online 11 November 2023

shaping future development trajectories of forests (Seidl and Turner, 2022). Predicting local light regimes is hence indispensable, especially as recent increases in forest disturbances are changing forest structure and demography (McDowell et al., 2020; Senf et al., 2021), likely leading to altered subcanopy light regimes in many forest ecosystems in the future.

Measuring light within forests is a challenging task, especially as the light availability in the understory of forests can be highly heterogeneous at a small spatial scale (Canham et al., 1990; Helbach et al., 2022). Direct approaches such as using handheld or stationary quantum sensors allow for measuring the amount of the incident solar radiation (Akitsu et al., 2017; Kutschera and Lamb, 2018), which is often quantified as the photosynthetically active part of the overall incident radiation (wavelengths from ~400 to ~700 nm), although other wavelengths in both the ionizing (Braga et al., 2015; Vanhaelewyn et al., 2020) as well as non-ionizing (Cserta et al., 2011; Kreye et al., 2018) domains can also have a considerable impact on forest ecosystems. While direct approaches yield an accurate representation of the light availability at a specific location and point in time, acquiring long-term datasets across large extents is costly. In contrast to direct methods, indirect approaches use models of various complexity to estimate the light availability in the understory of forests. Process-based or physical models, for instance, precisely describe the incident solar radiation and its interaction with the vegetation by physical functions (Brunner, 1998; Courbaud et al., 2003; Ligot et al., 2014). Those models, however, are difficult to parameterize and demanding regarding the computational resources needed in their application, which limits their utility for predicting subcanopy light regimes across large spatial extents. Empirical models, in turn, use statistical relationships between observed on-site conditions and the measured subcanopy light availability. The subcanopy light availability is thereby often described as the direct sunlight and diffuse illumination at the measurement location in proportion to a completely unshaded site (Behling, 2022; Canham, 1988; Canham et al., 1990). Yet, many variables describing on-site conditions being used as predictors in statistical models to predict the subcanopy light regime are often not available across large spatial extents (e.g., stand information derived from forest inventories) or over extended periods of time (e.g., to make inferences on the effects of changes in land cover). Estimating the subcanopy light regime across large spatial extents and monitoring it's change over time thus remains a challenging task.

Remote sensing offers novel ways forward in mapping, monitoring and understanding forest light regimes, as it enables cost-efficient, repeatable and large scale analyses. With respect to light regimes, Light Detection and Ranging (LiDAR) data is especially useful, because of its capability to characterize forest structures in great detail (Donager et al., 2021; Lim et al., 2003; Seidel et al., 2020). In fact, several studies have used LiDAR to map light regimes in the understory of forests (Seidel et al., 2012; Webster et al., 2020; Zellweger et al., 2019). While ALS can be considered the gold standard for mapping forest light regimes, it also has several drawbacks: First, ALS data is costly to acquire and many regions thus lack adequate coverage. Second, ALS data quality can vary widely and many ALS acquisitions are flown leaf-off to facilitate the computation of digital terrain models. Many locally calibrated or trained ALS based light models thus lack generality and are not transferable to other regions. Third, repeated ALS acquisitions are rare, limiting the ability to track changes in light availability over time using ALS.

To overcome these limitations of ALS data, novel spaceborne sensor systems, such as offered by the Copernicus Program of the European Space Agency, hold considerable potential. Data from the Sentinel-1 and Sentinel-2 satellite missions, for instance, might provide information on forest structure from space and thus enable a seamless monitoring of subcanopy forest light regimes across space and time. Sentinel-1 is operating in the microwave domain (wavelength center at ~ 5.55 cm) at ~ 10 *m* spatial resolution for different polarizations (dual HH + HV, VV + VH or single HH, VV), with a theoretical revisit time of six days for Sentinel-1 A and B for the ground range detected interferometric wide swath product (European Space Agency, 2022a). We note, however, that Sentinel-1 B quit service end of 2021, doubling the revisit time beyond that date (European Space Agency, 2022b). Microwave data can deliver information related to the dielectric properties and structural components of vegetation (Bae et al., 2019; Bruggisser et al., 2021; Dostálová et al., 2016), which is known to be highly correlated to the light regime (Lieffers et al., 1999; Messier et al., 1998; Montgomery and Chazdon, 2001). Sentinel-2 in turn, is a multispectral sensor system operating from the visible (VIS) to the shortwave-infrared (SWIR) wavelength domain. It provides a spatial resolution from ~10 *m* to ~20 m (~60 *m* for three atmospheric bands) with a theoretical revisit time of five days when combining Sentinel-2 A and B (European Space Agency, 2012, 2022c). While single images at a medium spatial resolution in the optical wavelength domain are limited in their ability to characterize forest structure (Camarretta et al., 2020; Cohen and Spies, 1992), an increasing number of images provide opportunities to glean information on structural properties, e.g., via photogrammetry (Pearse et al., 2018) or time series analysis (Pflugmacher et al., 2012). Sentinel-2 has the advantage of a relatively high temporal resolution that allows for characterizing intra-annual variability in spectral reflectance properties, often called spectral-temporal metrics or phenometrics. Those spectral-temporal metrics can be used to identify forest communities (Grabska et al., 2019; Hemmerling et al., 2021), which are linked to characteristic forest structural properties that in turn determine light regimes. The high temporal resolution of Sentinel-2 might thus compensate for sensor saturation and a lack of penetration depth in the optical wavelength domain. Furthermore, Sentinel-2 offers a higher spatial resolution than similar sensor systems in the optical wavelength domain (e.g., Landsat, MODIS), which allows for a more precise characterization of local crown structures and forest gaps (e.g., ~10 *m* is the typical crown width of a single adult tree in Central Europe). Yet, there is no study to date that tested the usability of Sentinel-1 and Sentinel-2 for mapping subcanopy light regimes of forest ecosystems, especially in comparison to the gold standard of ALS.

Here, our aim was to test the performance of spaceborne satellite data from Sentinel-1 and Sentinel-2 for mapping and monitoring subcanopy light regimes during leaf-on conditions in mountain forest landscapes of Central Europe, a challenging environment where light regimes vary significantly with changing forest communities along the elevation gradient. More specifically, our objectives were to: (1) compare Sentinel-1/2 time series against ALS data in their ability to predict the local subcanopy light regime during leaf-on conditions (as represented by the total site factor [TSF], a variable combining direct and diffuse light close to the forest floor); and to (2) test whether Sentinel-1/2 time series are better suited for making generalized predictions across study regions than local ALS data, evaluating their applicability for monitoring subcanopy light regimes in forest ecosystems across large spatial extents.

2. Data and methods

2.1. Study sites and plots

In our study we focused on mountain landscapes, because the incident solar radiation (and associated microclimatic warming effects) are of particular importance for vegetation under the harsh, temperature-limited conditions in mountain areas. We selected three different study sites in the Bavarian Alps in Germany: (A) Berchtesgaden, with ~92 km^2 of forest, (B) Karwendel with ~48 km^2 of forest and (C) Chiemgau with ~61 km^2 of forest (Fig. 1). While the first study site was used for model calibration and validation, the latter two study sites were used for testing the ability of our models to generalize and make predictions at realistic conditions in terms of data availability and quality. These study sites were thus not used for model calibration. All study sites are characterized by a high topographic complexity and a large

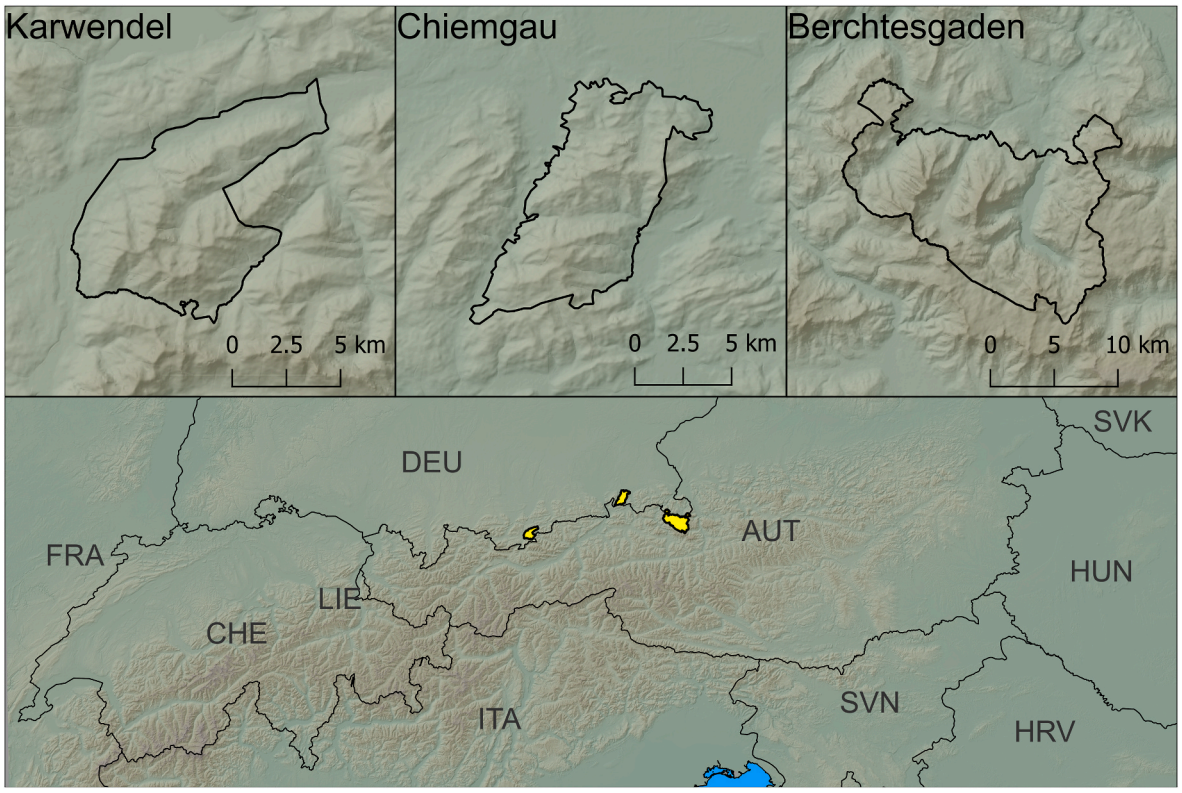

Fig. 1. Overview of the study sites along the Northern Alps in Bavaria, Germany.

elevation gradient, ranging from 535 *m* to 2713 *m* a.s.l. (with the tree line approximately at 1700 *m* a.s.l.). The average annual precipitation ranges from ~1100 to >2000 mm (Bayerisches Landesamt für Wasserwirtschaft, 1998) and the average annual temperature ranges from ~0 to 10 °C (Bayrisches Landesamt für Umwelt, 2020). Both temperature and precipitation vary considerably along elevational gradients. Soils range from bare, calcareous bedrock over weakly developed soils (Lithic Leptosol and Rendzic Leptosol) to mature soils (Cambisols) (Landesamt für Umwelt Bayern, 2022). Mixed forest communities prevail at lower elevations and are primarily composed of European beech (*Fagus sylvatica* L.) and to smaller parts of silver fir (*Abies alba* Mill.) and Norway spruce (*Picea abies* (L.) H. Karst.) (submontane forests, 500–850 *m* a.s.l.). With increasing elevation, the composition first shifts towards a stronger dominance of Norway spruce (montane forests, 850–1400 *m* a.s.l.), with subalpine forests (1400–1800 *m* a.s.l.) being characterized by a mix of Norway spruce, European larch (*Larix decidua* Mill.) and Swiss stone pine (*Pinus cembra* L.). The abundance of Norway spruce was increased by past forest management practices. Dwarf mountain pine (*Pinus mugo* Turra) is a shrub species occurring at the tree line (~1700–1800 *m* a.s.l.). While management has been ceased on 75% of the area for the calibration site Berchtesgaden (IUCN category II; national park), the study sites Karwendel and Chiemgau are actively managed with the main goal of multi-purpose forest management and a particular focus on sustaining the protective function of forests against natural hazards.

2.2. Light measurements for model calibration and validation

For model calibration and validation, we established a total of 150 plots of 500 m^2 (~12.6 *m* radius) at the calibration site Berchtesgaden. To adequately represent the highly variable site conditions, plot locations were stratified over five forest development stages (Gap, Establishment, Optimum, Plenter, Decay; cf. (Zenner et al., 2016); identified using existing forest inventory data) and three altitudinal belts (submontane, montane, subalpine). For each of the $3 \times 5 = 15$ combinations, 10 plots were established. These plot locations were geolocated with a state-of-the-art R12i global navigation satellite system of Trimble Inc (precision <1 *m* for 67 % of the plots, <2 *m* for all plots). To measure the local subcanopy light regime at each plot, we used a Solariscope SOL300 (Behling, 2022), which takes hemispherical photos and sets automatically applied thresholds along a gradient of brightness levels (seven thresholds in total) in order to distinguish vegetation from clear sky. The total site factor (TSF) is calculated from a hemispherical photo, as a user-defined ratio of the direct site factor (DSF; the direct sunlight reaching the measurement point) and the indirect site factor (ISF; the diffuse illumination at the measurement point). In our case, the TSF was calculated with a 60:40 ratio of DSF:ISF and the TSF indicates the percentage of light availability relative to a completely open site (e.g. open space or above canopy) (Anderson, 1964). The DSF time span was set to the vegetation period for the temperate climate zone (01.04.-30.09.) and an angle of view of 60° was chosen to determine the opening (Behling, 2022). A total of five measurements were conducted at a fixed height of 2 *m* above ground at each plot location: the first measurement was taken at the central plot coordinate and the other four measurements were taken in each cardinal direction from the central coordinate in a fixed distance of 10 m (Appendix 1). We decided for a measurement height of 2 *m* to capture the subcanopy light regime without the often dense understory vegetation layer. Following these measurements, three different interpreters evaluated all Solariscope measurements independently and selected the most appropriate of the seven available brightness thresholds for each hemispherical photo (Appendix 1). For this selection process, a threshold can be considered as ideal when sky-covering objects (e.g. leaves, branches, stems, etc.) can be perfectly discriminated from the open sky on the hemispherical photo (Behling, 2022). The TSF of the most frequently selected threshold was taken as final measurement. In cases of substantial deviation (≥0.03) between interpreters, a re-evaluation of the hemispherical photo was carried out (27% of all cases). As the final response variable used in our analyses, an averaged TSF was calculated over the five measurements for each plot

location. Light measurements were sampled July/August 2021 for the calibration site Berchtesgaden, June 2022 for the test site Karwendel and May 2022 for the test site Chiemgau.

2.3. Airborne laser scanning data and processing

A variety of continuously improving ALS sensor systems are available today, gathering three-dimensional information on forest ecosystems. Based on the availability across our study sites, we used ALS data of different topicality and quality for the three study sites. The ALS data for Berchtesgaden originated from an aerial survey flown with a Riegl VQ-780i scanner in September 2021 that was contracted by the national park authorities. The minimal point cloud resolution of this data is 30 points/m^2, it is already pre-classified (ground, non-ground and erroneous), and comes with intensity values. The ALS data for the independent test sites Karwendel and Chiemgau were provided by the Bavarian State Office for Survey and Geoinformation and have a minimal point density of 4 points/m^2. The datasets were acquired during several aerial surveys; for the test site Karwendel in August 2016 with a Riegl LMS-Q780 scanner and for the test site Chiemgau from August 2015 to January 2017 with a Riegl LMS-Q1560 scanner. Also these datasets were pre-classified (ground, non-ground, erroneous and build-up), but came without intensity values (Landesamt für Digitalisierung, Breitband und Vermessung, 2022).

For model calibration and validation we used a binary forest mask at 10 *m* spatial resolution available for the calibration site Berchtesgaden (Mandl, 2020) to calculate a set of metrics from the ALS data for all pixels classified as forest. For doing so, we retrieved the central pixel coordinates of each cell of the 10 *m* forest mask to subset the ALS point cloud with a radius of 15 *m* around this central pixel coordinate (slightly larger than the actual plot size to avoid edge effects in the following processing steps). After filtering for valid points using an isolated voxel filter, we took advantage of the point cloud classification and filtered point clouds to more than 5% not classified as water or ground. Subsequently, we normalized the point cloud based on ground classified points and a triangulated irregular network interpolation and subset it to the final plot size (i.e., 500 m^2, with a radius $\sim$ 12.56 *m*). From the subset normalized point cloud we calculated a canopy height model using the pit-free algorithm (Khosravipour et al., 2014). Furthermore, we voxelized the normalized point cloud to a spatial resolution of 0.1 *m*. These two datasets, the canopy height model and the voxelized and normalized point cloud, were then used to calculate the final ALS metrics. In total, we calculated 52 different metrics (Appendix 2). These metrics describe the vegetation structure at the plot locations in terms of overall density, height of the canopy, vertical and horizontal canopy distribution, as well as gap structure. To calculate the ALS based metrics, we relied on the R packages lidR, ForestGapR, spatstat. core and mgcv (Baddeley et al., 2022; Roussel, 2023; Roussel et al., 2020; Silva, 2023; Silva et al., 2019; Wood, 2017.

2.4. Sentinel-1 data and processing

We acquired all available Sentinel-1 Ground Range Detected data from 2021 via Google Earth Engine (European Space Agency, 2023; Gorelick et al., 2017). This data is already pre-processed based on ESA's Sentinel-1 Toolbox, including the following processing steps: an application of the orbit file, border- and thermal-noise removal as well as radiometric calibration and range doppler terrain correction with the digital elevation model of the Shuttle Radar Topography Mission (European Space Agency, 2022d; Farr et al., 2007). The data was further filtered for vertical-vertical (VV) and vertical-horizontal (VH) transmitter-receiver polarization in interferometric wide mode in both, ascending and descending orbits for the year 2021. The data represents the backscatter coefficient (sigma nought or σ0) in decibels of the target backscattering area (normalized radar cross-section) with a spatial resolution of ~10 *m*. After downloading and filtering the Sentinel-1 data, we applied a routine for angular-based, radiometric slope correction, optimized for volume scattering on the Sentinel-1 timeseries, to account for the distinct topography of our study sites (Vollrath et al., 2020). As digital elevation model, we used the Shuttle Radar Topographic Mission dataset, which is available on Google Earth Engine with a spatial resolution of ca. 30 *m* and an extent stretching from -60° to $+60^\circ$, not limiting the applicability of our developed approach to a specific region (Farr et al., 2007). For some pixels, no statistics could be calculated because of the sensor geometry of Sentinel-1 resulting in layover and shadow effects, thus leading to invalid pixel values. We did not use any buffer to mask further potentially invalid pixels in the border areas of layover and shadow effects. To reduce speckle without losing spatial resolution, we aggregated the pre-processed Sentinel-1 timeseries per pixel and built a median and mean composite for the summer season (July, August, September), winter season (December, January, February) as well as for the whole year for both, VV and VH polarization, as proposed in a previous study (Bae et al., 2019). We did not convert logarithmic transformed values ($10 \times \log10(x)$) into original values beforehand and the pixel values thus do not represent information in any physically unit. As our aim was at predicting using a machine learning tool, this does not affect downstream analysis. After converting the temporal composites to the desired coordinate reference system, we resampled them with our master raster layer for the respective study site using a nearest neighbor interpolation. Finally, we calculated 38 pixel-wise metrics based on the different composites (Appendix 2). Those metrics comprised of standard metrics, e.g. mean, median, difference, sum and ratio of the different polarizations for the temporal composites, as well as the Canopy Development Index (CDI), Radar Vegetation Index (RVI) and modified Radar Forest Degradation Index (mRFDI). In previous studies, the CDI and variations of it have proven useful to capture phenological information on deciduous forests (Bae et al., 2022; Frison et al., 2018). We calculated the CDI defined as σ0VV – σ0VH for all our temporal composites. Several variations exist also for the RVI. Originally, the quad-polarized RVI was introduced to estimate the level of biomass for agricultural applications (Kim and van Zyl, 2009; Yihyun Kim et al., 2012). Later, the RVI was first adapted for dual-polarization (Trudel et al., 2012) and then also used for forestry applications (Schulz et al., 2022). We here defined the RVI as $4\sigma0VH/(\sigma0VV + \sigma0VH)$ and calculated it for all our temporal composites. The Radar Forest Degradation Index (RFDI) was developed to discriminate different vegetation types (Mitchard et al., 2012). Originally, it requires a HH and VH polarization. However, since Sentinel-1 does only provide a VV and VH polarization, it was modified based on the assumption that the HH polarization corresponds to the VV polarization and hence can be used instead (Nasirzadehdizaji et al., 2019; Nicolau et al., 2021). We thus calculated the mRFDI for all our temporal composites defined as $(\sigma0VV - \sigma0VH)/(\sigma0VV + \sigma0VH)$.

2.5. Sentinel-2 data and processing

We acquired all available Sentinel-2, Level-1C data from the years 2019–2021 via the Google Cloud service. We used three years instead of just one year to account for high cloud cover at the study sites, which would result in unreliable estimates with only few, non-randomly distributed observations within one year. The downloaded data represents top-of-atmosphere reflectance with a spatial resolution from ~10 *m* to ~20 *m*, depending on the spectral band. Following the download, we processed the data using the Framework for Operational Radiometric Correction for Environmental monitoring (FORCE), including atmospheric correction to bottom-of-atmosphere, topographic- and radiometric-correction, as well as cloud masking (Frantz, 2019). Using all cloud-free pixels, we calculated a set of commonly used spectral indices: the Normalized Difference Vegetation Index (NDVI) (Lange et al., 2017; Tucker, 1979), the Enhanced Vegetation Index (EVI) (Hui Qing Liu and Huete, 1995), the Normalized Burn Ratio (NBR) (Key and Benson, 2006), the Soil Adjusted Vegetation Index (SAVI) (Huete, 1988),

the Tasseled Cap Greenness (TC-Green), Wetness (TC-Wet), and Brightness (TC-Bright) components (Crist and Cicone, 1984; Kauth and Thomas, 1976), the Normalized Difference Water Index (NDWI) (Gao, 1996), and the Normalized Difference Moisture Index (NDMI) (Hardisky et al., 1983; Vogelmann and Rock, 1988). From these indices, various pixelwise statistics (i.e., mean, standard deviation, minimum, maximum, range, various quantiles, interquartile range, skewness, kurtosis) for the entire years of 2019–2021 were calculated, resulting in a total of 108 metrics (Appendix 2). As a last step, also this data was converted into the desired coordinate reference system and resampled with our master raster layer for the respective study site using a nearest neighbor interpolation just like we did for the Sentinel-1 data.

2.6. Predicting light regimes

We used the above-described metrics from ALS, Sentinel-1, Sentinel-2 and a combination of Sentinel-1/2 to model the observed TSF at the 150 plot locations of the calibration site Berchtesgaden. To identify the most important predictor variables from the overall large number of metrics for each model, we used a stepwise variable selection approach implemented in the R package VSURF that builds upon permutation of the random forest variable importance measure (Genuer et al., 2015). After variable selection, we used the random forest algorithm with the R package caret to set up the final models. We set the final number of trees to 10,000 and used a 10-fold cross-validation to evaluate the model performance using the root mean squared error (RMSE) and squared Pearson correlation coefficient (R^2) as measures of model performance. The number of variables used for each split was selected using the approach implemented in the R package caret (i.e., two for the ALS and the Sentinel-2 based model, and five for the Sentinel-1 and Sentinel-1/2 based model) (Kuhn, 2008). Subsequently, we used the calibrated models to predict the TSF across the full forest area at 10 *m* spatial resolution.

2.7. Comparing model performance and testing model generalizability

We compared the produced maps for the calibration site Berchtesgaden with one another by calculating differences between the best spaceborne prediction and the prediction based on ALS data (i.e., our gold standard reference). Non-available pixels, resulting from cloud cover, layover- and shadow-effects were masked for all predictions. We further compared the maps across topographic gradients, investigating whether the strong topography (in terms of both, elevation and slope) of our study site influences spatial predictions of the TSF.

To test the generalization performance of our fitted models to new sites, we investigated their performance at the independent test sites Karwendel and Chiemgau, which were not used for model calibration before. To that end we sampled 50 additional plots in each of these two study sites. Since no forest inventories for these study sites were available to reproduce the stratification applied for the calibration site Berchtesgaden, a random forest model was trained on the calibration site Berchtesgaden to predict the five forest development stages also for the test sites Karwendel and Chiemgau. As input for this model, we used the standard metrics from the R package lidR (Roussel et al., 2020) and the ALS data as described in Section 2.3. Using a road-/trail-map to guarantee accessibility, we selected plot locations accessible in the field but spanning a wide gradient of elevation zones. Despite careful planning, five plot locations remained inaccessible at the test site Karwendel and were thus dropped from the sample. For each of the remaining 95 plot locations we recorded the TSF in the field as described above with hemispherical photography. We calculated the same metrics for the ALS data as well as for the Sentinel-1/2 data as for the calibration site Berchtesgaden. In a next step, we used the models fitted for the calibration site Berchtesgaden and the calculated metrics to predict the TSF for the test sites Karwendel and Chiemgau. We then compared the predictions with the TSF measurements at the plot locations for these two test sites. To account for the possibility of forest disturbances occurring between light measurements and ALS acquisition, we used an existing disturbance map (Senf and Seidl, 2021) to filter out plot locations that were disturbed between ALS acquisitions and light measurements.

3. Results

The best performing model for the calibration site Berchtesgaden was the model based on ALS variables with a R^2 of 0.90 and a RMSE/MAE of 0.08/0.06. The performances of the Sentinel-1 model (R^2 of 0.39 and a RMSE/MAE of 0.20/0.17) as well as the Sentinel-2 model (R^2 of 0.72 and a RMSE/MAE of 0.13/0.11) were lower. However, the model based on a combination of Sentinel-1/2 variables also performed well, with a R^2 of 0.80 and a RMSE/MAE of 0.11/0.09. The lower accuracy of the Sentinel-based models is visible in the scatterplots shown in the left column of Fig. 2. The ALS model has the narrowest spread around the 1:1 line, followed by the combined Sentinel-1/2 model. Comparing the cross-validated model residuals over elevation and slope did not reveal any distinct trends, suggesting that the accuracy of the predicted TSF is consistent over the reference sample (Fig. 2, columns 2, 3).

3.1. Predictor variables

Among all models, the ALS model used the lowest number of predictor variables: only four out of 52 predictor variables were sufficient for modelling the TSF from ALS (Table 1). The most important predictor variable was the ratio between the percentage of returns above 2 m (i.e., the height at which the Solariscope measurements were conducted) to the total number of returns, representing the overall canopy density at the plot locations. Further important predictor variables for the ALS model were the 0.25 and the 0.5 quantile of the canopy height model (CHM), describing the vertical characteristics of the canopy. Lastly, the averaged area of gaps within the CHM at 5 *m* height emerged as important predictor variable, describing the horizontal heterogeneity at a plot location.

A total of eight predictor variables were important for the Sentinel-1 model (Table 1). These predictor variables were mainly incorporating different combinations of the VV and VH polarization and were complemented by mean and median composites of the VV polarization for the entire year. Regarding the seasonality of the composites, we could not identify any trend: both, the summer and the winter composites were of importance for predicting the TSF.

The Sentinel-2 model was also based on eight predictor variables (Table 1), which without exception included the NIR band at 842 nm and almost always the Shortwave Infrared (SWIR) bands at 940 nm and 1375 nm. Furthermore, nearly all selected predictor variables were based on the median (0.5 quantile), whereas high or low quantiles contained little additional information of value for the model.

For the model combining predictor variables of Sentinel-1/2, nine predictor variables were selected as important. Although the performance of the model based on Sentinel-1 solely was rather low, two predictor variables of Sentinel-1 were included into the joint model, enhancing the prediction accuracy over the model solely based on Sentinel-2 metrics. Yet, Sentinel-2 predictor variables were overall more important in the joint model.

3.2. Predicted subcanopy light availability for the calibration site berchtesgaden

The spatial predictions of the TSF for the calibration site Berchtesgaden from the two best performing models (i.e., ALS and Sentinel-1/2) showed similar patterns overall (Fig. 3), while some important differences remained (Figs. 4 and 5). For both sets of predictions, the light availability increased with elevation, confirming the general expectation for mountain forests that forest cover and canopy density decreases with increasing elevation. On average, predicted TSF values increased

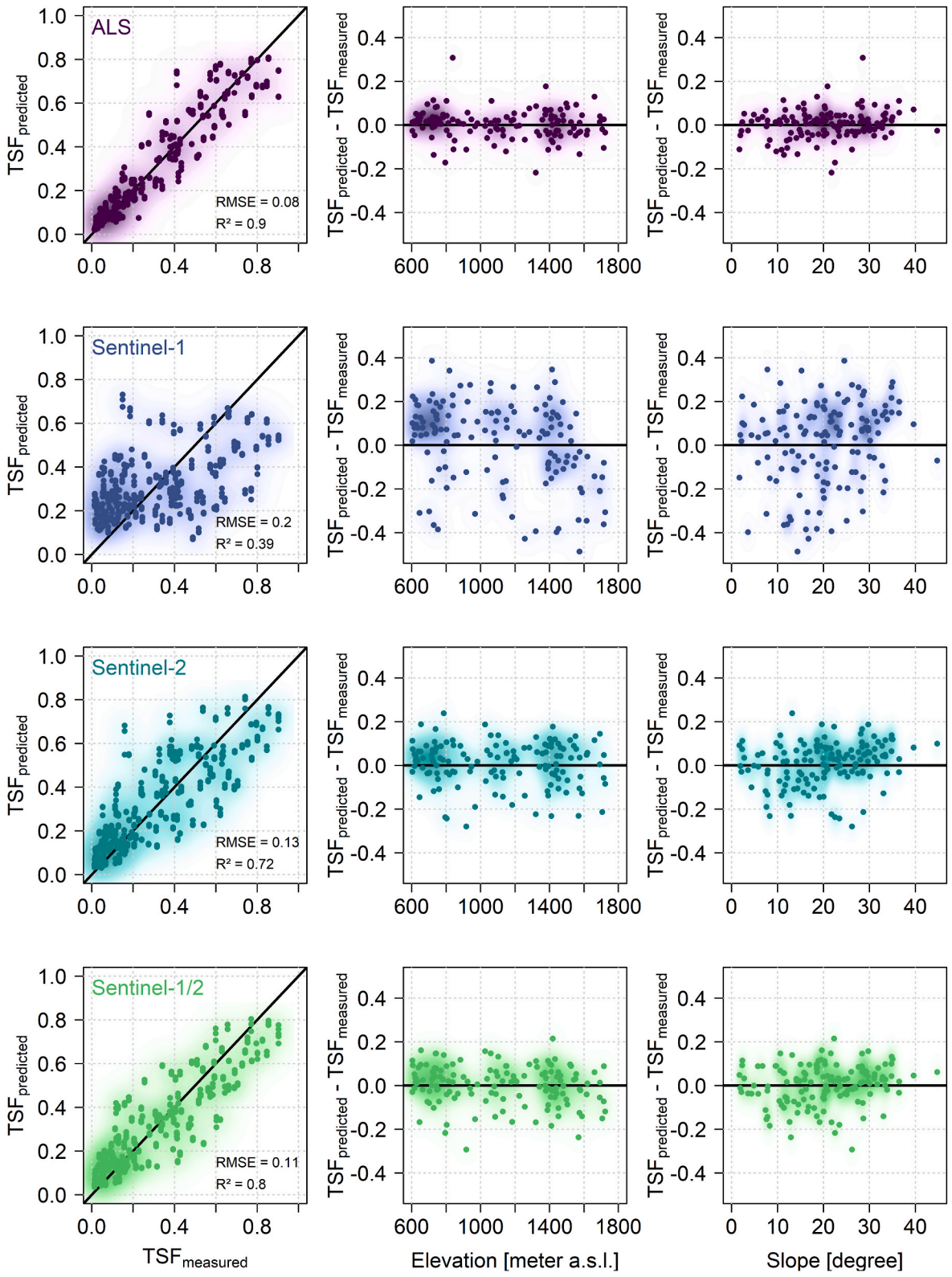

Fig. 2. First column: Total Site Factor (TSF) measured versus predicted based on a 10-fold cross validation for the calibration site Berchtesgaden. The solid line represents the 1:1 line (TSF measured = TSF predicted). Second column: Elevation a.s.l. Versus cross-validated model-residuals. Third column: Slope versus cross-validated model-residuals. The density of all points is illustrated by the intensity of the color code selected for the specific models. (For interpretation of the references to color in this figure legend, the reader is referred to the Web version of this article.)

Table 1
Predictor variables, their importance and model performance for the four models predicting the Total Site Factor (TSF) from Airborne Laser Scanning (ALS), Sentinel-1, Sentinel-2 and a combination of Sentinel-1/2 data. The ranking indicates the scaled predictor variable importance of the random forest models as defined in the R package *randomForest* (Breiman, 2001). Details on predictor variables can be found in Appendix 2.

Model:	Predictor variables:	Scaled variable importance:	R^2	RMSE	MAE
ALS	PtsAbove2m	100.00	0.90	0.08	0.06
	CHM_Q025	83.39			
	CHMGapArea5m_Mean	19.68			
	CHM_Q050	0.00			
Sentinel-1	S1_mRFDI_Winter_Mean	100.00	0.39	0.20	0.17
	S1_VV_VH_Ratio_Winter_Mean	96.04			
	S1_VV_Summer_Median	42.09			
	S1_VV_Year_Mean	39.93			
	S1_VV_VH_Sum_Year_Mean	28.07			
	S1_VV_VH_Sum_Summer_Median	21.80			
	S1_CDI_Summer_Mean	12.58			
	S1_VV_Year_Median	0.00			
Sentinel-2	S2_NDWI_Q050	100.00	0.72	0.13	0.11
	S2_NDVI_Q075	83.20			
	S2_NBR_Q050	66.43			
	S2_TCW_Q050	56.69			
	S2_NDWI_Q010	31.49			
	S2_TCW_Mean	6.42			
	S2_NDMI_Q050	0.8			
	S2_TCW_Q050	0.00			
Sentinel-1/2	S2_NBR_Q050	100	0.80	0.11	0.09
	S2_NDWI_Q050	81.01			
	S2_TCW_Q050	49.23			
	S2_NDVI_Q075	34.48			
	S1_VV_VH_Sum_Year_Median	14.85			
	S2_NDWI_Q010	9.54			
	S2_TCW_Mean	8.80			
	S1_VV_VH_Sum_Year_Mean	7.99			
	S2_NDMI_Q050	0.00			

by 0.03 per 100 *m* elevation gain for both the ALS model and the Sentinel-1/2 model, suggesting that both models well represent the overall elevation gradient in subcanopy light availability.

Across all forests of the calibration site Berchtesgaden, we predicted an averaged TSF of 0.32 and 0.34 with the ALS model and Sentinel-1/2 model, respectively. For the ALS model, the 5% and 95% quantiles of the predicted TSF were 0.06 and 0.72, whereas they were 0.07 and 0.68 for the Sentinel-1/2 model. This information confirms the visual impression (Fig. 3) that the range of the predicted TSF values from the ALS model is slightly larger than the range of the predicted TSF values from the Sentinel-1/2 model, leading to a somewhat finer graduation in predicted TSF values for the ALS model. A direct comparison of the spatial TSF predictions from the ALS and Sentinel-1/2 models showed a high correlation ($r = 0.69$) between both maps. Yet, the model based on Sentinel-1/2 predicts on average 2% higher TSF values than the ALS model. This overestimation of the TSF can be mainly attributed to areas with steep slopes (i.e., $>45^\circ$ in slope angle, such as at the western banks of lake Königssee in the center of Fig. 5). Such slopes are beyond the range of values contained in our 150 training plots (cf. Fig. 2). However, only 11.36% of all pixels with TSF predictions had a slope $\geq 45^\circ$, rendering overestimation in steep slopes a relatively minor problem across the landscape. Comparing the spatial predictions of the TSF to high resolution true color imagery (Landesamt für Digitalisierung, 2023), we found that fine structured forest patches and pixels bordering non-forest landcover types were less accurately represented by the Sentinel-1/2 model compared to the ALS model (Fig. 5). Small features below or close to the spatial resolution of the spaceborne systems (i.e., very small gaps, narrow gulleys, skid trails) were also represented insufficiently and thus deviated from the ALS based prediction (Figs. 4 and 5).

3.3. Predicted subcanopy light availability for the study sites Karwendel and Chiemgau

For the test sites Karwendel and Chiemgau the performance of the fitted models was more variable. Both sites were not used for model calibration and the resolution of the ALS data was much lower than for the calibration site Berchtesgaden. For the test site Karwendel, the Sentinel-1/2-model outperformed the ALS model, with a R^2 of 0.67 (and a RMSE/MAE of 0.13/0.08), compared to a R^2 of 0.61 (and a RMSE/MAE of 0.13/0.11) (Fig. 6). That is, model accuracies for the ALS model decreased by 0.29 points when generalizing the model to a new site, combined with a decrease in point cloud resolution by a factor of ~ 7. For the test site Chiemgau, the ALS model performed better than the Sentinel-1/2 model, with a R^2 of 0.79 (and a RMSE/MAE of 0.11/0.08) compared to a R^2 of 0.67 (and a RMSE/MAE of 0.15/0.09). Yet, also here the accuracy of the ALS model was considerably lower than at the calibration site Berchtesgaden. In contrast, generalization performance for the Sentinel-1/2 model was consistent across study sites, with similar accuracies for both independent test sites and a constant decrease of 0.14 points in R^2 when applying the model to a new site.

4. Discussion

Here, we present a first benchmark of spaceborne remote sensing for mapping subcanopy light regimes in temperate mountain forests, by comparing it to ALS data as the gold standard for mapping forest light. Our results confirm the notion that subcanopy light regimes can be mapped from ALS data with high accuracies. The good performance of ALS for predicting subcanopy light regimes can be explained by the potential of ALS to quantify forest structural information (Donager et al., 2021; Lim et al., 2003; Seidel et al., 2020), which is tightly linked to the subcanopy light regime of forests (Alexander et al., 2013; Seidel et al., 2012; Webster et al., 2020; Zellweger et al., 2019). The most important

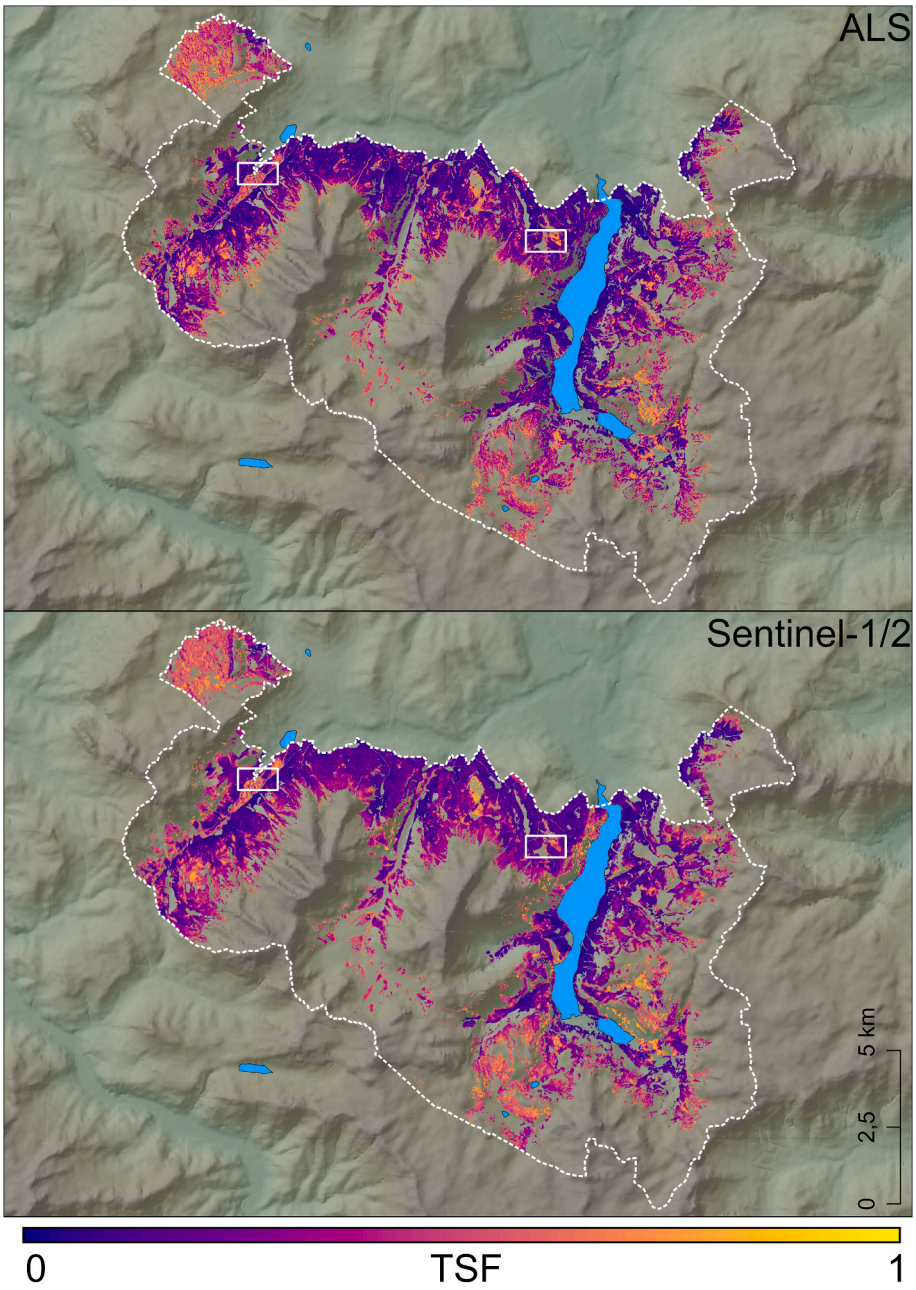

Fig. 3. Predicted Total Site Factor (TSF) values for the study site Berchtesgaden for all forest pixels for the ALS model (upper panel) and the Sentinel-1/2 model (lower panel). The white boxes denote the subsets reported in Fig. 6.

predictor variable in the ALS model was overall canopy cover (i.e., PtsAbove2m), calculated as the ratio between the percentage of returns above 2 *m* to the total number of returns, and thus indicative of the amount of sun shading leaves, branches and stems. Being calculated as a ratio, the PtsAbove2m variable was robust to the resolution of the point cloud. In contrast, predictor variables describing the horizontal characteristics/heterogeneity of the forest canopy (i.e., CHMGapArea5m_Mean) are likely to be more sensitive to the resolution of the point cloud. The gap structure of the canopy is, however, also identified as an important predictor variable, with small gaps leading to more light reaching the forest floor locally, even when the overall canopy cover is moderate or high. Finally, we found the 25% and 50% quantiles of the CHM to be relevant in predicting subcanopy light regimes with ALS. Based on previous studies, both variables can be seen as a proxy for forest development stages (Falkowski et al., 2009), which are strong determinants of the subcanopy light regime. Overall, our study confirms that ALS data is well-suited for modelling subcanopy light regimes, with parsimonious models of relatively few predictor variables (four in our case) allowing for accurate models.

Our results also demonstrate the potential of spaceborne data from the optical- and micro-wavelength domain (i.e., Sentinel-1/2) to map subcanopy light regimes. However, Sentinel-2 performed better than Sentinel-1 alone. The most important predictor variables derived from Sentinel-2 characterized the average conditions in vegetation incorporating the SWIR reflectance (i.e., S2_NBR_Q050, S2_TCW_Q050, S2_NDMI_Q050). Spectral indices based on the SWIR are sensitive to leaf water content and leaf structure (Ceccato et al., 2001), leaf area (Cohen and Goward, 2004; Lee et al., 2004), to the structure of forest canopies and to forest age (Cohen et al., 1995; Horler and Ahern, 1986) as well as above ground biomass in general (Chen et al., 2018; Chrysafis et al., 2017; Grabska and Socha, 2021). The importance of a range of SWIR based indices might thus be first and foremost related to their ability to

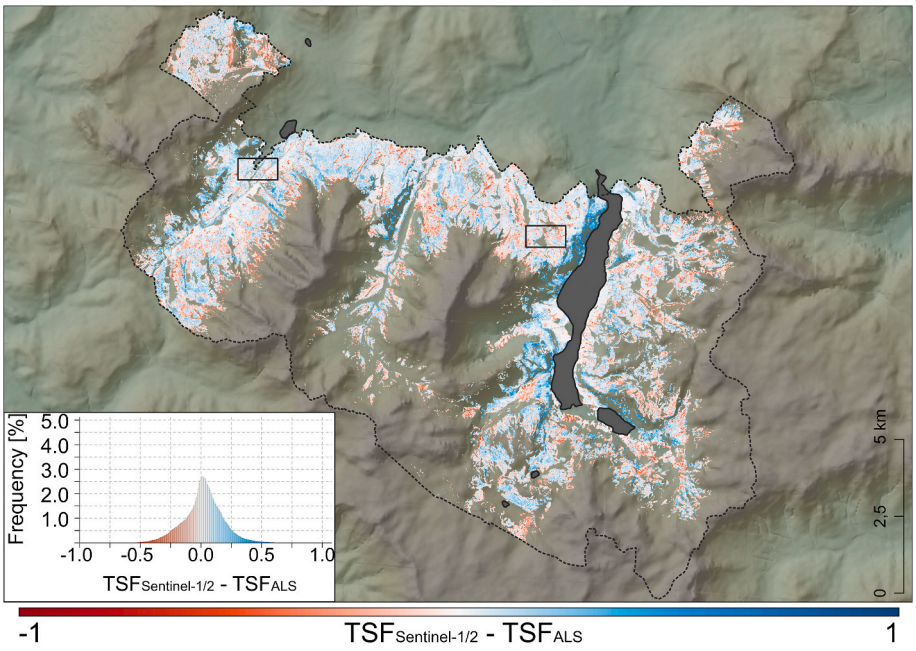

Fig. 4. Difference of the predicted Total Site Factor (TSF) values for the Sentinel-1/2 model and the ALS model. Red pixels represent an underestimation, blue pixels an overestimation of the predicted TSF values by the Sentinel-1/2 model compared to the ALS model. The black boxes illustrate the subsets used in Fig. 5. (For interpretation of the references to color in this figure legend, the reader is referred to the Web version of this article.)

characterize tree canopy structures better than indices based on NIR or visible bands (Cohen et al., 1995; Cohen and Goward, 2004). The informative value of SWIR-based indices for characterizing the tree canopy is also reflected in their widespread use for detecting forest disturbances, where SWIR-based indices are significantly better in detecting canopy gaps than indices based on visible and NIR bands (Cohen et al., 2018; Healey et al., 2005, 2006). SWIR-based indices – especially at a 10 *m* spatial resolution as provided by Sentinel-2 – are thus likely also indicative of canopy gaps leading to a higher subcanopy light availability. Interestingly, predictor variables describing the intra-annual variation in spectral reflectance (i.e., the standard deviation or lower and upper quantiles) were not among the most important predictor variables. This might be attributed back to the fact that we trained our models based on measurements of the local light regime at peak growing season and the related phenological information, despite its ability to discriminate forest communities (Grabska et al., 2019; Hemmerling et al., 2021; Sheeren et al., 2016), seems to be less important. That said, we found both, the 10 % quantile of NDVI and the 75 % quantile of NDVI to be important predictor variables, which might indicate their ability to discriminate between coniferous and broad-leaved stands and their different subcanopy light regimes.

Including radar data further improved the prediction of subcanopy light regimes. The predictor variables selected for the final models presented the sum of the mean and median backscatter signal per pixel for the VV and VH polarization from Sentinel-1 over the entire year (i.e., S1_VV_VH_Sum_Year_Mean and S1_VV_VH_Sum_Year_Median). The backscatter signal depends on sensor-specific properties (e.g., local incidence angle, wavelength, polarization etc.) as well as on ground specific properties, comprising topography (slope and aspect) and land cover with its dielectric and structural properties. Previous studies found a high correlation between NDVI and the ratio of VV and VH polarization for both croplands (Veloso et al., 2017) and forests (Frison et al., 2018). Consequently, the sum of the backscatter signal from the VV and VH polarization could increase with higher biomass, due to seasonality at varying rates however for different forest communities, for which we also expect diverging subcanopy light regimes. Overall, we found that the fusion of Sentinel-1 and Sentinel-2 was best able to predict subcanopy forest light regimes from space, suggesting that the information of both sensor systems is complementary.

Despite the overall good performance of the Sentinel-1/2 model methodological challenges remain. First, we observed that the light values predicted by the Sentinel-1/2 model had a smaller range than the values predicted by the ALS model. This suggests that data from Sentinel-1/2 do not represent extreme cases well, compared to ALS data. A further reason for a lower range of predicted light values is the well-known saturation effects for both, Sentinel-1/2, and the lower spatial resolution of spaceborne data compared to the airborne data. Radar sensor systems like Sentinel-1, working with shorter micro-wavelengths e.g., *X*-band or *C*-band, saturate faster than sensor systems operating at longer micro-wavelengths e.g., L-band or *P*-band, due to their limited penetration depth (Huang et al., 2018; Imhoff, 1995). Similar effects are documented for data of the optical-wavelength domain recorded by Sentinel-2, which also saturates with increasing vegetation density (Carlson and Ripley, 1997; Chen et al., 2018; Gamon et al., 1995; Lu et al., 2016; Meyer et al., 2019). Likewise, open areas might have dense understory vegetation that is difficult to separate spectrally from trees. This can lead to an underestimation of the local light availability by optical data compared to ALS data, which allows the separation of understory vegetation and overstory trees by means of height information.

A methodological point of consideration is the compositing of Sentinel-1 data, for which images from both ascending and descending orbits have been used. By aggregating many images over time, speckle effects could be reduced without losing spatial resolution. Yet, the information contained in the aggregated backscatter signal is blurred due to the effects of different orbit parameters (e.g., diverging local incidence angles), in combination with the complex topography of our study sites. This might also partly explain the lower predictive performance of Sentinel-1 in our study. First attempts to provide normalized Sentinel-1 data from different orbits exist, but availability of this data is still limited to specific regions or periods of time (Bauer-Marschallinger et al., 2021). Finally, the lower spatial resolution of Sentinel-1/2 likely also adds to the lower predictive performance of spaceborne systems. While the 10 *m* resolution of Sentinel-1/2 is already high compared to other spaceborne sensor systems (e.g., Landsat, MODIS), canopy gaps below the spatial resolution will remain difficult to detect from space, while they are reflected in ALS point clouds. This became especially evident when

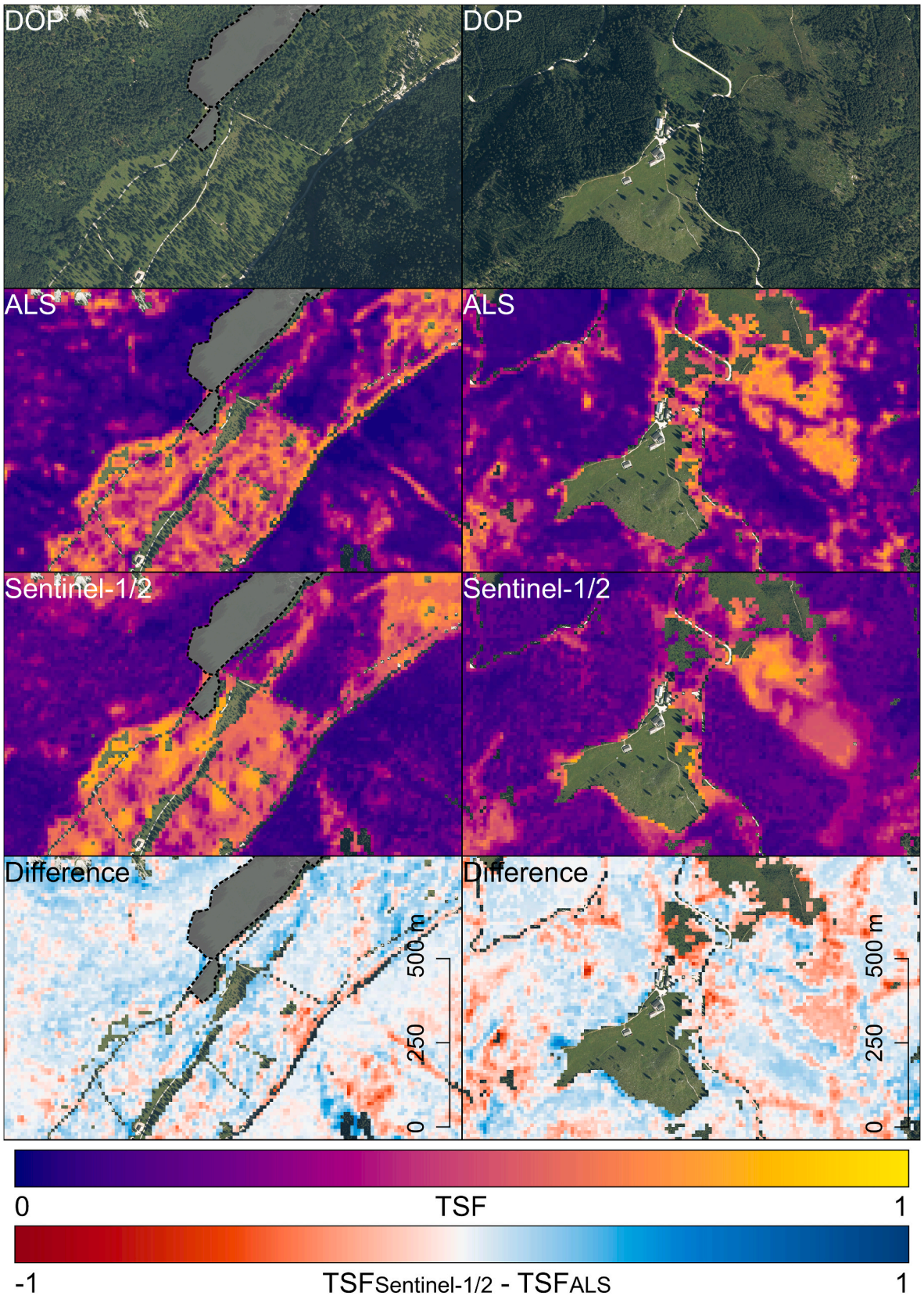

Fig. 5. Predicted Total Site Factor (TSF) values and the difference for the ALS model and the Sentinel-1/2 model for two subsets of the calibration site Berchtesgaden, selected for their heterogeneous forest cover. Predictions and differences are only shown for forested pixels. Note that a temporal offset of approximately one and a half years exists between the datasets used to predict light availability and the high-resolution, true color digital orthophoto (DOP) commissioned by the Agency for Digitisation, High-Speed Internet and Surveying of the federal state Bavaria (Landesamt für Digitalisierung, Breitband und Vermessung, 2023). (For interpretation of the references to color in this figure legend, the reader is referred to the Web version of this article.)

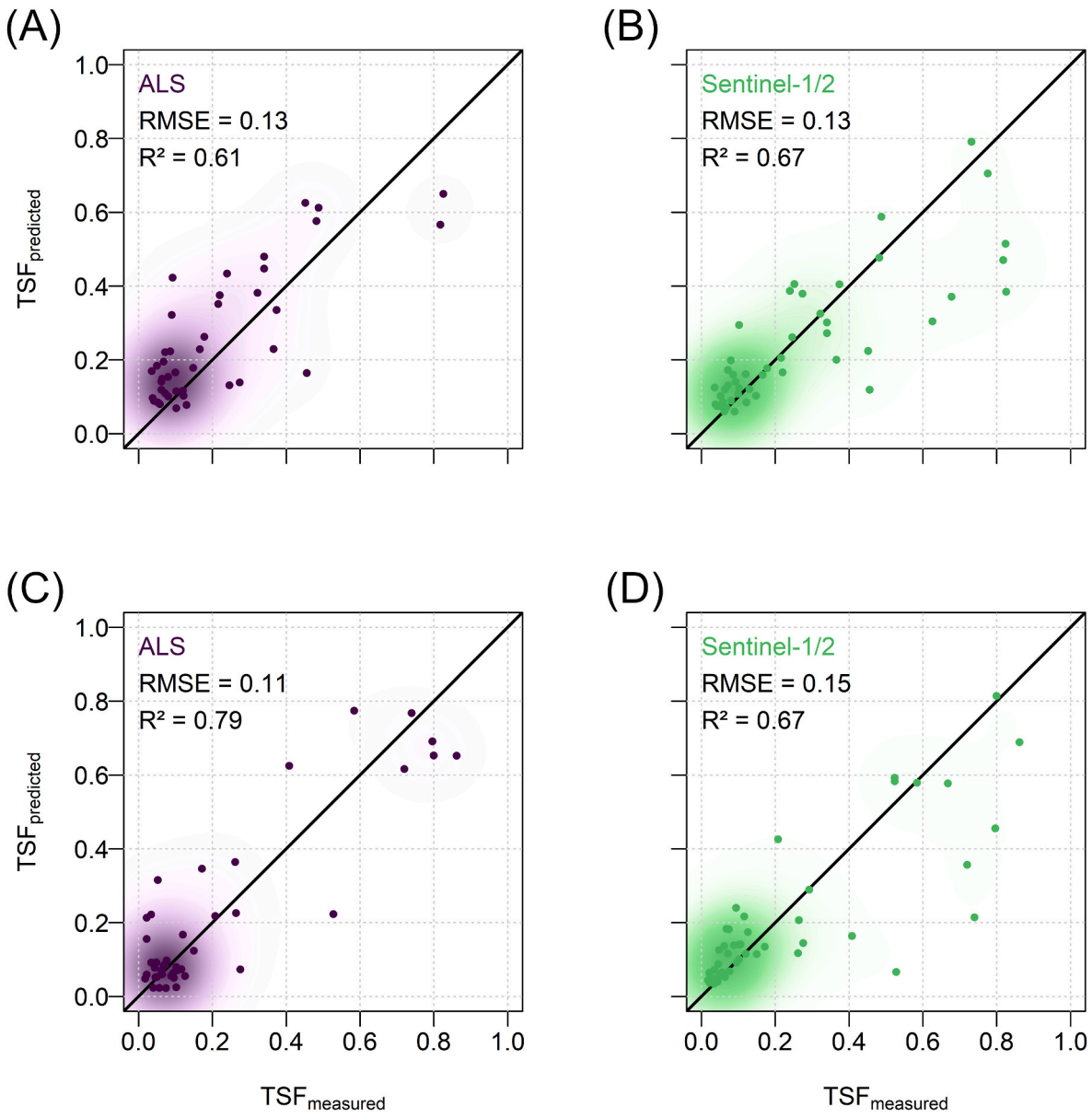

Fig. 6. Total Site Factor (TSF) measured versus TSF predicted for the test sites Karwendel by the ALS model (A) and by the Sentinel-1/2 model (B) and for the test site Chiemgau by the ALS model (C) and by the Sentinel-1/2 model (D). The density of all points is illustrated by the intensity of the respective color code. (For interpretation of the references to color in this figure legend, the reader is referred to the Web version of this article.)

comparing our maps with high resolution true color imagery (Fig. 5), where small gaps, narrow gullies and skid trails were often not well represented in Sentinel-1/2 model predictions. This effect might be further exaggerated by geolocation inaccuracies of ~12.5 *m* for Sentinel-2 (Clerc et al., 2021; Gascon et al., 2017) and of ~ 2.4 *m* for Sentinel-1 (Charles, 2021), which were likely amplified by pre-processing of the data. A recent study, for instance, highlights the offset between vegetation height and digital terrain model used for pre-processing, leading to an inaccurate topographic and radiometric correction of the backscatter signal for Sentinel-1 (Zehner et al., 2023) This might also explain the stronger disagreement between the ALS-based and Sentinel-1/2-based predictions for very steep slopes (>45°) (Appendix 3). Furthermore, the topographic correction applied to Sentinel-1 only represents a simplified, angular relationship between acquired radar images and topography (Hoekman and Reiche, 2015; Small, 2011; Vollrath et al., 2020). The digital elevation model itself used for topographic correction (Shuttle Radar Topography Mission) might also introduce possible errors due to a temporal offset of several years and a relatively lower spatial resolution (Farr et al., 2007).

The ALS model performed better than the Sentinel-1/2 model for the calibration site Berchtesgaden, for which we had up-to-date, high-quality ALS data. However, when considering a realistic application scenario (i.e., here represented by the two independent test sites Karwendel and Chiemgau), the superiority of ALS over Sentinel-1/2 was less clear. ALS data for the test sites Karwendel and Chiemgau were both older, of lower quality and partly recorded in a different season (leaf-off season for test site Chiemgau), which led to a substantially lower performance of the ALS model for both test sites compared to the calibration site Berchtesgaden (it should be however mentioned that for our two test sites Karwendel and Chiemgau plot locations with a high measured TSF are rare and the validation for this range of values thus has limited explanatory power). Previous studies found that different measurement conditions (e.g., seasonality, wind, fog, etc.) can drastically influence calculated ALS metrics, especially when point cloud resolution decreases (Côté et al., 2011; Liang et al., 2016; Mathes et al., 2023). For the Sentinel-1/2 model, however, model performance

remained more or less constant when applying the model trained on the calibration site to the two test sites. We attribute the higher generalization power of Sentinel-1/2 to two aspects already mentioned above: First, the temporal offset between ALS and field data acquisition, which can lead to differences in areas when forest characteristics changes (i.e., for both application sites, for instance, we had to remove ten plots that had been disturbed between ALS acquisition and the field measurement campaign). Second, the point cloud resolution of the data is much lower for our test sites, which – as discussed above – will increase the uncertainty in prominent ALS based metrics (e.g., gap fraction). For the Sentinel-1/2 model, we benefitted from freely available data which is consistent in terms of both actuality and quality. This allows to generalize models trained in one site to new sites, as we show here. Using free and open archives of spaceborne data thus opens up the possibility for mapping subcanopy light regimes over long temporal and large spatial extents, such as the temporal monitoring of changes in leaf-on subcanopy light regimes in response to natural disturbances and forest management (Frolking et al., 2009; Hilker et al., 2009; Senf and Seidl, 2021), or large-scale spatial prediction at national or even continental scales for parameterizing and/or evaluating ecosystem models (De Bruijn et al., 2014; Lischke et al., 2006; Rammer and Seidl, 2019; Schumacher et al., 2004). Future research could also investigate the possibility of spaceborne data to assess within-year changes in subcanopy light regimes, that is differences in light regimes between leaf-on and leaf-off conditions.

5. Conclusion

Monitoring subcanopy forest light – which is a major driver of plant growth and vegetation composition at the forest floor – is a crucial task for better understanding forest ecosystems. In this study, we compared the potential of Sentinel-1/2 to predict the subcanopy light regimes to ALS data – the current gold standard in assessing forest structure and biophysical processes. We show that up-to-date high-resolution ALS data yields highest accuracies in predicting subcanopy light regimes, but that Sentinel-1 and Sentinel-2 time series perform almost equally well. The limited availability of up-to-date and high-quality ALS data hinders generalizability and application to new regions, which is possible with Sentinel-1/2. Our results thus demonstrate the feasibility to use Sentinel-1 and Sentinel-2 for monitoring the subcanopy light regime across large spatial and long temporal extents. This has important implications for the operational monitoring of forest ecosystems, which often relies on challenging to acquire airborne datasets.

Author contributions

FG, CS, RS and PA conceived the study idea. CS and RS planned and organized the data collection, with help of FG and PA. FG analyzed the data, with help of CS and PA. FG and CS wrote the paper, with revision from RS and PA.

Declaration of competing interest

The authors declare that they have no known competing financial interests or personal relationships that could have appeared to influence the work reported in this paper.

Data availability

Data will be made available on request.

Acknowledgements

This work was funded by the Bavarian State Ministry for Food, Agriculture and Forestry (StMELF) in the frame of the project “Erarbeitung, Umsetzung und Evaluierung von wildökologischen Zonierungskonzepten” (Project Nr. JA-17). R.S. acknowledges support from the European Research Council under the European Space Agency, 2012 research and innovation program (Grant Agreement 101001905). We thank Thomas Jagdhuber and his colleagues for their helpful remarks processing the Sentinel-1 data. Furthermore, we thank Martin Süß, Michael Lukasser, Leon Mahlkow, Max Malten and Robin Reiter for their help with fieldwork.

Appendix A. Supplementary data

Supplementary data to this article can be found online at https://doi.org/10.1016/j.srs.2023.100107.

References

Akitsu, T., Nasahara, K.N., Hirose, Y., Ijima, O., Kume, A., 2017. Quantum sensors for accurate and stable long-term photosynthetically active radiation observations. Agric. For. Meteorol. 237–238, 171–183. https://doi.org/10.1016/j.agrformet.2017.01.011.

Alexander, C., Moeslund, J.E., Bøcher, P.K., Arge, L., Svenning, J.-C., 2013. Airborne laser scanner (LiDAR) proxies for understory light conditions. Remote Sens. Environ. 134, 152–161. https://doi.org/10.1016/j.rse.2013.02.028.

Anderson, M.C., 1964. Studies of the woodland light climate: I. The photographic computation of light conditions. J. Ecol. 52, 27–41. https://doi.org/10.2307/2257780.

Baddeley, A., Jalilian, A., Rubak, E., Fend, C., Waagepetersen, R., 2022. spatstat.core.

Bae, S., Levick, S.R., Heidrich, L., Magdon, P., Leutner, B.F., Wöllauer, S., Serebryanyk, A., Nauss, T., Krzystek, P., Gossner, M.M., Schall, P., Heibl, C., Bässler, C., Doerfler, I., Schulze, E.-D., Krah, F.-S., Culmsee, H., Jung, K., Heurich, M., Fischer, M., Seibold, S., Thorn, S., Gerlach, T., Hothorn, T., Weisser, W. W., Müller, J., 2019. Radar vision in the mapping of forest biodiversity from space. Nat. Commun. 10, 4757. https://doi.org/10.1038/s41467-019-12737-x.

Bae, S., Müller, J., Förster, B., Hilmers, T., Hochrein, S., Jacobs, M., Leroy, B.M.L., Pretzsch, H., Weisser, W.W., Mitesser, O., 2022. Tracking the temporal dynamics of insect defoliation by high-resolution radar satellite data. Methods Ecol. Evol. 13, 121–132. https://doi.org/10.1111/2041-210X.13726.

Bauer-Marschallinger, B., Cao, S., Navacchi, C., Freeman, V., Reuß, F., Geudtner, D., Rommen, B., Vega, F.C., Snoeij, P., Attema, E., Reimer, C., Wagner, W., 2021. The normalised Sentinel-1 Global Backscatter Model, mapping Earth’s land surface with C-band microwaves. Sci. Data 8, 277. https://doi.org/10.1038/s41597-021-01059-7.

Bayerisches Landesamt für Wasserwirtschaft, 1998. Mittlerer Jahresniederschlag in Bayern (Periode 1961-1990 [WWW Document]. URL. https://www.lfu.bayern.de/wasser/hydrometerologische_parameter/hydrometeorologie_auswertung/niederschlag/doc/karte_niederschlag.pdf, 3.20.23.

Bayrisches Landesamt für Umwelt, 2020. Mittlere Jahrestemperatur in Bayern. Referenzperiode 1971 - 2000) [WWW Document]. Bayrisches Klimainformationssystem. URL. https://klimainformationssystem.bayern.de/klimatool/klimatool-der-vergangenheit, 3.20.20.

Behling, R., 2022. Solariscope SOL 300 - Reference Manual.

Braga, G.U.L., Rangel, D.E.N., Fernandes, É.K.K., Flint, S.D., Roberts, D.W., 2015. Molecular and physiological effects of environmental UV radiation on fungal conidia. Curr. Genet. 61, 405–425. https://doi.org/10.1007/s00294-015-0483-0.

Breiman, L., 2001. Random forests. Mach. Learn. 45, 5–32. https://doi.org/10.1023/A:1010933404324.

Bruggisser, M., Dorigo, W., Dostálová, A., Hollaus, M., Navacchi, C., Schlaffer, S., Pfeifer, N., 2021. Potential of Sentinel-1 C-band time series to derive structural parameters of temperate deciduous forests. Rem. Sens. 13, 798. https://doi.org/10.3390/rs13040798.

Brunner, A., 1998. A light model for spatially explicit forest stand models. For. Ecol. Manag. 107, 19–46. https://doi.org/10.1016/S0378-1127(97)00325-3.

Camarretta, N., Harrison, P.A., Bailey, T., Potts, B., Lucieer, A., Davidson, N., Hunt, M., 2020. Monitoring forest structure to guide adaptive management of forest restoration: a review of remote sensing approaches. New Fed. 51, 573–596. https://doi.org/10.1007/s11056-019-09754-5.

Canham, C.D., 1988. An index for understory light levels in and around canopy gaps. Ecology 69, 1634–1638. https://doi.org/10.2307/1941664.

Canham, C.D., Denslow, J.S., Platt, W.J., Runkle, J.R., Spies, T.A., White, P.S., 1990. Light regimes beneath closed canopies and tree-fall gaps in temperate and tropical forests. Can. J. For. Res. 20, 620–631. https://doi.org/10.1139/x90-084.

Carlson, T.N., Ripley, D.A., 1997. On the relation between NDVI, fractional vegetation cover, and leaf area index. Remote Sens. Environ. 62, 241–252. https://doi.org/10.1016/S0034-4257(97)00104-1.

Ceccato, P., Flasse, S., Tarantola, S., Jacquemoud, S., Grégoire, J.-M., 2001. Detecting vegetation leaf water content using reflectance in the optical domain. Remote Sens. Environ. 77, 22–33. https://doi.org/10.1016/S0034-4257(01)00191-2.

Charles, P., 2021. S-1A & S-1B Annual Performance Report for 2021.

Chen, Y., Li, L., Lu, D., Li, D., 2018. Exploring bamboo forest aboveground biomass estimation using sentinel-2 data. Rem. Sens. 11, 7. https://doi.org/10.3390/rs11010007.

Chrysafis, I., Mallinis, G., Siachalou, S., Patias, P., 2017. Assessing the relationships between growing stock volume and Sentinel-2 imagery in a Mediterranean forest

ecosystem. Remote Sens. Lett. 8, 508–517. https://doi.org/10.1080/2150704X.2017.1295479.
Clerc, S., Devignot, O., Pessiot, L., 2021. S2 MPC - L1C Data Quality Report.
Cohen, W.B., Goward, S.N., 2004. Landsat's role in ecological applications of remote sensing. Bioscience 54, 535. https://doi.org/10.1641/0006-3568(2004)054[0535:LRIEAO]2.0.CO;2.
Cohen, W.B., Spies, T.A., 1992. Estimating structural attributes of Douglas-fir/western hemlock forest stands from landsat and SPOT imagery. Remote Sens. Environ. 41, 1–17. https://doi.org/10.1016/0034-4257(92)90056-.
Cohen, W.B., Spies, T.A., Fiorella, M., 1995. Estimating the age and structure of forests in a multi-ownership landscape of western Oregon. U.S.A. Int. J. Remote Sens. 16, 721–746. https://doi.org/10.1080/01431169508954436.
Cohen, W.B., Yang, Z., Healey, S.P., Kennedy, R.E., Gorelick, N., 2018. A LandTrendr multispectral ensemble for forest disturbance detection. Remote Sens. Environ. 205, 131–140. https://doi.org/10.1016/j.rse.2017.11.015.
Côté, J.-F., Fournier, R.A., Egli, R., 2011. An architectural model of trees to estimate forest structural attributes using terrestrial LiDAR. Environ. Model. Software 26, 761–777. https://doi.org/10.1016/j.envsoft.2010.12.008.
Courbaud, B., de Coligny, F., Cordonnier, T., 2003. Simulating radiation distribution in a heterogeneous Norway spruce forest on a slope. Agric. For. Meteorol. 116, 1–18. https://doi.org/10.1016/S0168-1923(02)00254-X.
Crist, E.P., Cicone, R.C., 1984. A physically-based transformation of thematic mapper data—the TM tasseled Cap. IEEE Trans. Geosci. Rem. Sens. GE-22, 256–263. https://doi.org/10.1109/TGRS.1984.350619.
Cserta, E., Hegedűs, G., Németh, R., 2011. Drying process in Norway spruce wood exposed to infrared radiation. Bioresources 6, 4181–4189. https://doi.org/10.15376/biores.6.4.4181-4189.
De Bruijn, A., Gustafson, E.J., Sturtevant, B.R., Foster, J.R., Miranda, B.R., Lichti, N.I., Jacobs, D.F., 2014. Toward more robust projections of forest landscape dynamics under novel environmental conditions: embedding PnET within LANDIS-II. Ecol. Model. 287, 44–57. https://doi.org/10.1016/j.ecolmodel.2014.05.004.
Donager, J.J., Sánchez Meador, A.J., Blackburn, R.C., 2021. Adjudicating perspectives on forest structure: how do airborne, terrestrial, and mobile lidar-derived estimates compare? Rem. Sens. 13, 2297. https://doi.org/10.3390/rs13122297.
Dormann, C.F., Bagnara, M., Boch, S., Hinderling, J., Janeiro-Otero, A., Schäfer, D., Schall, P., Hartig, F., 2020. Plant species richness increases with light availability, but not variability, in temperate forests understorey. BMC Ecol. 20, 43. https://doi.org/10.1186/s12898-020-00311-9.
Dostálová, A., Milenković, M., Hollaus, M., Wagner, W., 2016. Influence of Forest Structure on the Sentinel-1 Backscatter Variation- Analysis with Full-Waveform LiDAR Data.
Europe, Forest, 2020. State of Europe's Forests - 2020 394.
European Space Agency, 2012. Sentinel-2 - ESA's optical high-resolution mission for GMES operational services [WWW Document]. URL. https://esamultimedia.esa.int/multimedia/publications/SP-1322_2/offline/download.pdf, 3.14.23.
European Space Agency, 2022a. Sentinel-1 SAR user guide [WWW Document]. Sentin. Online. URL. https://sentinels.copernicus.eu/web/sentinel/user-guides/sentinel-1-sar, 11.1.22.
European Space Agency, 2022b. Mission ends for Copernicus sentinel-1B satellite [WWW Document]. URL. https://www.esa.int/Applications/Observing_the_Earth/Copernicus/Sentinel-1/Mission_ends_for_Copernicus_Sentinel-1B_satellite, 3.13.23.
European Space Agency, 2022c. Sentinel-2 MSI Technical Guide [WWW Document]. Sentin. Online. URL. https://sentinels.copernicus.eu/web/sentinel/technical-guides/sentinel-2-msi, 11.1.22.
European Space Agency, 2022d. SNAP - ESA Sentinel Application Platform.
European Space Agency, 2023. Ground range detected - sentinel-1 - SAR technical guide [WWW Document]. URL. https://sentinels.copernicus.eu/web/sentinel/technical-guides/sentinel-1-sar/products-algorithms/level-1-algorithms/ground-range-detected, 1.31.23.
Falkowski, M.J., Evans, J.S., Martinuzzi, S., Gessler, P.E., Hudak, A.T., 2009. Characterizing forest succession with lidar data: an evaluation for the Inland Northwest, USA. Remote Sens. Environ. 113, 946–956. https://doi.org/10.1016/j.rse.2009.01.003.
FAO, 2022. In: Forest Pathways for Green Recovery and Building Inclusive, Resilient and Sustainable Economies, State of the World's Forests. FAO, Rome. https://doi.org/10.4060/cb9360en.
Farr, T.G., Rosen, P.A., Caro, E., Crippen, R., Duren, R., Hensley, S., Kobrick, M., Paller, M., Rodriguez, E., Roth, L., Seal, D., Shaffer, S., Shimada, J., Umland, J., Werner, M., Oskin, M., Burbank, D., Alsdorf, D., 2007. The Shuttle radar topography mission. Rev. Geophys. 45, RG2004. https://doi.org/10.1029/2005RG000183.
Frantz, D., 2019. FORCE—landsat + sentinel-2 analysis ready data and beyond. Rem. Sens. 11, 1124. https://doi.org/10.3390/rs11091124.
Frison, P.-L., Fruneau, B., Kmiha, S., Soudani, K., Dufrêne, E., Toan, T.L., Koleck, T., Villard, L., Mougin, E., Rudant, J.-P., 2018. Potential of sentinel-1 data for monitoring temperate mixed forest phenology. Rem. Sens. 10, 2049. https://doi.org/10.3390/rs10122049.
Frolking, S., Palace, M.W., Clark, D.B., Chambers, J.Q., Shugart, H.H., Hurtt, G.C., 2009. Forest disturbance and recovery: a general review in the context of spaceborne remote sensing of impacts on aboveground biomass and canopy structure. J. Geophys. Res. Biogeosciences 114. https://doi.org/10.1029/2008JG000911.
Gamon, J.A., Field, C.B., Goulden, M.L., Griffin, K.L., Hartley, A.E., Joel, G., Penuelas, J., Valentini, R., 1995. Relationships between NDVI, canopy structure, and photosynthesis in three californian vegetation types. Ecol. Appl. 5, 28–41. https://doi.org/10.2307/1942049.
Gao, B., 1996. NDWI—a normalized difference water index for remote sensing of vegetation liquid water from space. Remote Sens. Environ. 58, 257–266. https://doi.org/10.1016/S0034-4257(96)00067-3.
Gascon, F., Bouzinac, C., Thépaut, O., Jung, M., Francesconi, B., Louis, J., Lonjou, V., Lafrance, B., Massera, S., Gaudel-Vacaresse, A., Languille, F., Alhammoud, B., Viallefont, F., Pflug, B., Bieniarz, J., Clerc, S., Pessiot, L., Trémas, T., Cadau, E., De Bonis, R., Isola, C., Martimort, P., Fernandez, V., 2017. Copernicus sentinel-2A calibration and products validation status. Rem. Sens. 9, 584. https://doi.org/10.3390/rs9060584.
Genuer, R., Poggi, J.-M., Tuleau-Malot, C., 2015. VSURF: an R package for variable selection. Using Random Forests 7, 16.
Giuggiola, A., Ogée, J., Rigling, A., Gessler, A., Bugmann, H., Treydte, K., 2016. Improvement of water and light availability after thinning at a xeric site: which matters more? A dual isotope approach. New Phytol. 210, 108–121. https://doi.org/10.1111/nph.13748.
Gorelick, N., Hancher, M., Dixon, M., Ilyushchenko, S., Thau, D., Moore, R., 2017. Google earth engine: planetary-scale geospatial analysis for everyone. Remote Sens. Environ. 202, 18–27. https://doi.org/10.1016/j.rse.2017.06.031.
Grabska, E., Socha, J., 2021. Evaluating the effect of stand properties and site conditions on the forest reflectance from Sentinel-2 time series. PLoS One 16, e0248459. https://doi.org/10.1371/journal.pone.0248459.
Grabska, E., Hostert, P., Pflugmacher, D., Ostapowicz, K., 2019. Forest stand species mapping using the sentinel-2 time series. Rem. Sens. 11, 1197. https://doi.org/10.3390/rs11101197.
Hardisky, M., Klemas, V., Smart, R., 1983. The influence of soil salinity, growth, form and leaf moisture on the spectral radiance of Spartina alterflora canopies. Photogramm. Eng. Rem. Sens. No. 1 77–83 https://www.asprs.org/wp-content/uploads/pers/1983journal/jan/1983_jan_77-83.pdf.
Hardwick, S.R., Toumi, R., Pfeifer, M., Turner, E.C., Reuben, N., Ewers, R.M., 2015. The relationship between leaf area index and microclimate in tropical forest and oil palm plantation: forest disturbance drives changes in microclimate. Agric. For. Meteorol. 201, 187–195. https://doi.org/10.1016/j.agrformet.2014.11.010.
Healey, S., Cohen, W., Zhiqiang, Y., Krankina, O., 2005. Comparison of Tasseled Cap-based Landsat data structures for use in forest disturbance detection. Remote Sens. Environ. 97, 301–310. https://doi.org/10.1016/j.rse.2005.05.009.
Healey, S.P., Yang, Z., Cohen, W.B., Pierce, D.J., 2006. Application of two regression-based methods to estimate the effects of partial harvest on forest structure using Landsat data. Remote Sens. Environ. 101, 115–126. https://doi.org/10.1016/j.rse.2005.12.006.
Heithecker, T.D., Halpern, C.B., 2006. Variation in microclimate associated with dispersed-retention harvests in coniferous forests of western Washington. For. Ecol. Manag. 226, 60–71. https://doi.org/10.1016/j.foreco.2006.01.024.
Helbach, J., Frey, J., Messier, C., Mörsdorf, M., Scherer-Lorenzen, M., 2022. Light heterogeneity affects understory plant species richness in temperate forests supporting the heterogeneity–diversity hypothesis. Ecol. Evol. 12 https://doi.org/10.1002/ece3.8534.
Hemmerling, J., Pflugmacher, D., Hostert, P., 2021. Mapping temperate forest tree species using dense Sentinel-2 time series. Remote Sens. Environ. 267, 112743 https://doi.org/10.1016/j.rse.2021.112743.
Hilker, T., Wulder, M.A., Coops, N.C., Linke, J., McDermid, G., Masek, J.G., Gao, F., White, J.C., 2009. A new data fusion model for high spatial- and temporal-resolution mapping of forest disturbance based on Landsat and MODIS. Remote Sens. Environ. 113, 1613–1627. https://doi.org/10.1016/j.rse.2009.03.007.
Hoekman, D.H., Reiche, J., 2015. Multi-model radiometric slope correction of SAR images of complex terrain using a two-stage semi-empirical approach. Remote Sens. Environ. 156, 1–10. https://doi.org/10.1016/j.rse.2014.08.037.
Horler, D.N.H., Ahern, F.J., 1986. Forestry information content of Thematic Mapper data. Int. J. Rem. Sens. 7, 405–428. https://doi.org/10.1080/01431168608954695.
Huang, X., Ziniti, B., Torbick, N., Ducey, M., 2018. Assessment of forest above ground biomass estimation using multi-temporal C-band sentinel-1 and polarimetric L-band PALSAR-2 data. Rem. Sens. 10, 1424. https://doi.org/10.3390/rs10091424.
Huete, A.R., 1988. A soil-adjusted vegetation index (SAVI). Remote Sens. Environ. 25, 295–309. https://doi.org/10.1016/0034-4257(88)90106-X.
Imhoff, M.L., 1995. A theoretical analysis of the effect of forest structure on synthetic aperture radar backscatter and the remote sensing of biomass. IEEE Trans. Geosci. Rem. Sens. 33, 341–351. https://doi.org/10.1109/TGRS.1995.8746015.
Kauth, R.J., Thomas, G., 1976. The Tasselled Cap–a Graphic Description of the Spectral-Temporal Development of Agricultural Crops as Seen by Landsat. Presented at the LARS symposia, p. 159.
Key, C., Benson, N., 2006. Landscape Assessment (LA): Sampling and Analysis Methods–Remote Sensing of Severity, the Normalized Burn Ratio. USDA Forest Service Gen. Tech. Rep. RMRS-GTR-164-CD, 2006. LA1-LA5.
Khosravipour, A., Skidmore, A.K., Isenburg, M., Wang, T., Hussin, Y.A., 2014. Generating pit-free canopy height models from airborne lidar. Photogramm. Eng. Rem. Sens. 80, 863–872. https://doi.org/10.14358/PERS.80.9.863.
Kim, Y., van Zyl, J.J., 2009. A time-series approach to estimate soil moisture using polarimetric radar data. IEEE Trans. Geosci. Rem. Sens. 47, 2519–2527. https://doi.org/10.1109/TGRS.2009.2014944.
Kim, Yihyun, Jackson, T., Bindlish, R., Lee, Hoonyol, Hong, Sukyoung, 2012. Radar vegetation index for estimating the vegetation water content of rice and soybean. Geosci. Rem. Sens. Lett. IEEE 9, 564–568. https://doi.org/10.1109/LGRS.2011.2174772.
Kimmins, J.P., 2004. Forest Ecology: a Foundation for Sustainable Forest Management and Environmental Ethics in Forestry, third ed. Prentice Hall, Upper Saddle River, N. J.

Kreye, J.K., Hiers, J.K., Varner, J.M., Hornsby, B., Drukker, S., O'Brien, J.J., 2018. Effects of solar heating on the moisture dynamics of forest floor litter in humid environments: composition, structure, and position matter. Can. J. For. Res. 48, 1331–1342. https://doi.org/10.1139/cjfr-2018-0147.

Kuhn, M., 2008. Building predictive models in R using the caret package. J. Stat. Software 28. https://doi.org/10.18637/jss.v028.i05.

Kutschera, A., Lamb, J.J., 2018. Light meter for measuring photosynthetically active radiation. Am. J. Plant Sci. 9, 2420–2428. https://doi.org/10.4236/ajps.2018.912175.

Landesamt für Digitalisierung, 2023. Breitband und Vermessung. Echtfarben-Orthophoto (RGB-DOP) 2020 [WWW Document]. Orthophotos - Entzerrte Maßstabsgetreue Luftbilder. URL. https://www.ldbv.bayern.de/produkte/luftbild/orthophotos.html, 1.24.23.

Landesamt für Digitalisierung, Breitband und Vermessung, 2022. Laserpunkte - erfassung der Geländeoberfläche vom Flugzeug aus [WWW Document]. URL. https://www.ldbv.bayern.de/produkte/3dprodukte/laser.html, 11.2.22.

Landesamt für Umwelt Bayern, 2022. Übersichtsbodenkarte 1:25.000 - LfU Bayern [WWW Document]. URL. https://www.lfu.bayern.de/boden/karten_daten/uebk25/index.htm, 1.16.23.

Lange, M., Dechant, B., Rebmann, C., Vohland, M., Cuntz, M., Doktor, D., 2017. Validating MODIS and sentinel-2 NDVI products at a temperate deciduous forest site using two independent ground-based sensors. Sensors 17, 1855. https://doi.org/10.3390/s17081855.

Lee, K.-S., Cohen, W.B., Kennedy, R.E., Maiersperger, T.K., Gower, S.T., 2004. Hyperspectral versus multispectral data for estimating leaf area index in four different biomes. Remote Sens. Environ. 91, 508–520. https://doi.org/10.1016/j.rse.2004.04.010.

Lettenmaier, L., Seibold, S., Bässler, C., Brandl, R., Gruppe, A., Müller, J., Hagge, J., 2022. Beetle diversity is higher in sunny forests due to higher microclimatic heterogeneity in deadwood. Oecologia 198, 825–834. https://doi.org/10.1007/s00442-022-05141-8.

Liang, X., Kankare, V., Hyyppä, J., Wang, Y., Kukko, A., Haggrén, H., Yu, X., Kaartinen, H., Jaakkola, A., Guan, F., Holopainen, M., Vastaranta, M., 2016. Terrestrial laser scanning in forest inventories. ISPRS J. Photogrammetry Remote Sens. 115, 63–77. https://doi.org/10.1016/j.isprsjprs.2016.01.006.

Lieffers, V., Messier, C., Stadt, K., Gendron, F., Comeau, P., 1999. Predicting and managing light in the understory of boreal forests. Can. J. For. Res. 29, 796–811.

Ligot, G., Balandier, P., Courbaud, B., Claessens, H., 2014. Forest radiative transfer models: which approach for which application? Can. J. For. Res. 44, 391–403. https://doi.org/10.1139/cjfr-2013-0494.

Lim, K., Treitz, P., Wulder, M., St-Onge, B., Flood, M., 2003. LiDAR remote sensing of forest structure. Prog. Phys. Geogr. Earth Environ. 27, 88–106. https://doi.org/10.1191/0309133303pp360ra.

Lischke, H., Zimmermann, N.E., Bolliger, J., Rickebusch, S., Löffler, T.J., 2006. TreeMig: a forest-landscape model for simulating spatio-temporal patterns from stand to landscape scale. Ecol. Model. 199, 409–420. https://doi.org/10.1016/j.ecolmodel.2005.11.046.

Liu, Hui Qing, Huete, A., 1995. A feedback based modification of the NDVI to minimize canopy background and atmospheric noise. IEEE Trans. Geosci. Rem. Sens. 33, 457–465. https://doi.org/10.1109/36.377946.

Lu, D., Chen, Q., Wang, G., Liu, L., Li, G., Moran, E., 2016. A survey of remote sensing-based aboveground biomass estimation methods in forest ecosystems. Int. J. Digit. Earth 9, 63–105. https://doi.org/10.1080/17538947.2014.990526.

Mandl, L., 2020. Standardized derivation of forest stands using LiDAR data. Nationalpark Berchtesgaden.

Mathes, T., Seidel, D., Häberle, K.-H., Pretzsch, H., Annighöfer, P., 2023. What are we missing? Occlusion in laser scanning point clouds and its impact on the detection of single-tree morphologies and stand structural variables. Rem. Sens. 15, 450. https://doi.org/10.3390/rs15020450.

McDowell, N.G., Allen, C.D., Anderson-Teixeira, K., Aukema, B.H., Bond-Lamberty, B., Chini, L., Clark, J.S., Dietze, M., Grossiord, C., Hanbury-Brown, A., Hurtt, G.C., Jackson, R.B., Johnson, D.J., Kueppers, L., Lichstein, J.W., Ogle, K., Poulter, B., Pugh, T.A.M., Seidl, R., Turner, M.G., Uriarte, M., Walker, A.P., Xu, C., 2020. Pervasive shifts in forest dynamics in a changing world. Science 368, eaaz9463. https://doi.org/10.1126/science.aaz9463.

Messier, C., Parent, S., Bergeron, Y., 1998. Effects of overstory and understory vegetation on the understory light environment in mixed boreal forests. J. Veg. Sci. 9, 511–520. https://doi.org/10.2307/3237266.

Meyer, L.H., Heurich, M., Beudert, B., Premier, J., Pflugmacher, D., 2019. Comparison of landsat-8 and sentinel-2 data for estimation of leaf area index in temperate forests. Rem. Sens. 11, 1160. https://doi.org/10.3390/rs11101160.

Mitchard, E.T.A., Saatchi, S.S., White, L.J.T., Abernethy, K.A., Jeffery, K.J., Lewis, S.L., Collins, M., Lefsky, M.A., Leal, M.E., Woodhouse, I.H., Meir, P., 2012. Mapping tropical forest biomass with radar and spaceborne LiDAR in Lopé National Park, Gabon: overcoming problems of high biomass and persistent cloud. Biogeosciences 9, 179–191. https://doi.org/10.5194/bg-9-179-2012.

Montgomery, R.A., Chazdon, R.L., 2001. Forest structure, canopy architecture, and light transmittance in tropical wet forests. Ecology 82, 2707–2718. https://doi.org/10.1890/0012-9658(2001)082[2707:FSCAAL]2.0.CO;2.

Nasirzadehdizaji, R., Balik Sanli, F., Abdikan, S., Cakir, Z., Sekertekin, A., Ustuner, M., 2019. Sensitivity analysis of multi-temporal sentinel-1 SAR parameters to crop height and canopy coverage. Appl. Sci. 9, 655. https://doi.org/10.3390/app9040655.

Nemani, R.R., Keeling, C.D., Hashimoto, H., Jolly, W.M., Piper, S.C., Tucker, C.J., Myneni, R.B., Running, S.W., 2003. Climate-driven increases in global terrestrial net primary production from 1982 to 1999. Science 300, 1560–1563. https://doi.org/10.1126/science.1082750.

Nicolau, A.P., Flores-Anderson, A., Griffin, R., Herndon, K., Meyer, F.J., 2021. Assessing SAR C-band data to effectively distinguish modified land uses in a heavily disturbed Amazon forest. Int. J. Appl. Earth Obs. Geoinformation 94, 102214. https://doi.org/10.1016/j.jag.2020.102214.

Oliver, C.D., Larson, B.A., 1996. Forest stand dynamics. In: Formerly Published by John Wiley & Sons; Copyright Now Held by C.D.Oliver & B.C. Larson, Update Edition. New York, NY.

Pearse, G.D., Dash, J.P., Persson, H.J., Watt, M.S., 2018. Comparison of high-density LiDAR and satellite photogrammetry for forest inventory. ISPRS J. Photogrammetry Remote Sens. 142, 257–267. https://doi.org/10.1016/j.isprsjprs.2018.06.006.

Pflugmacher, D., Cohen, W.B., Kennedy, R.E., 2012. Using Landsat-derived disturbance history (1972–2010) to predict current forest structure. Remote Sens. Environ. 122, 146–165. https://doi.org/10.1016/j.rse.2011.09.025.

Rammer, W., Seidl, R., 2019. A scalable model of vegetation transitions using deep neural networks. Methods Ecol. Evol. 10, 879–890. https://doi.org/10.1111/2041-210X.13171.

Ritter, E., Dalsgaard, L., Einhorn, K.S., 2005. Light, temperature and soil moisture regimes following gap formation in a semi-natural beech-dominated forest in Denmark. For. Ecol. Manag. 206, 15–33. https://doi.org/10.1016/j.foreco.2004.08.011.

Roussel, J.-R., 2023. lidR: Airborne LiDAR Data Manipulation and Visualization for Forestry Applications. documentation), D.A. (Reviews the, features), F.D.B. (Fixed bugs and improved catalog, segment_snags, A.S.M. (Implemented wing2015 for, track_sensor), B.J.-F. (Contributed to R. for, track_sensor), G.D. (Implemented G. for, management), L.S. (Contributed to parallelization, code), S.A. (Author of the C. concaveman.

Roussel, J.-R., Auty, D., Coops, N.C., Tompalski, P., Goodbody, T.R.H., Meador, A.S., Bourdon, J.-F., de Boissieu, F., Achim, A., 2020. lidR: an R package for analysis of Airborne Laser Scanning (ALS) data. Remote Sens. Environ. 251, 112061 https://doi.org/10.1016/j.rse.2020.112061.

Schmidt, M., Jochheim, H., Kersebaum, K.-C., Lischeid, G., Nendel, C., 2017. Gradients of microclimate, carbon and nitrogen in transition zones of fragmented landscapes – a review. Agric. For. Meteorol. 232, 659–671. https://doi.org/10.1016/j.agrformet.2016.10.022.

Schulz, C., Förster, M., Vulova, S., Gränzig, T., Kleinschmit, B., 2022. Exploring the temporal fingerprints of mid-European forest types from sentinel-1 RVI and sentinel-2 NDVI time series. In: IGARSS 2022 - 2022 IEEE International Geoscience and Remote Sensing Symposium. Presented at the IGARSS 2022 - 2022 IEEE International Geoscience and Remote Sensing Symposium, pp. 5563–5566. https://doi.org/10.1109/IGARSS46834.2022.9884173.

Schumacher, S., Bugmann, H., Mladenoff, D.J., 2004. Improving the formulation of tree growth and succession in a spatially explicit landscape model. Ecol. Model. 180, 175–194. https://doi.org/10.1016/j.ecolmodel.2003.12.055.

Seidel, D., Fleck, S., Leuschner, C., 2012. Analyzing forest canopies with ground-based laser scanning: a comparison with hemispherical photography. Agric. For. Meteorol. 154–155, 1–8. https://doi.org/10.1016/j.agrformet.2011.10.006.

Seibold, Sebastian, Bässler, Claus, Brandl, Roland, Büche, Boris, Szallies, Alexander, Thorn, Simon, Ulyshen, Michael D., Müller, Jörg, 2016. Microclimate and habitat heterogeneity as the major drivers of beetle diversity in dead wood. J. Appl. Energy. https://doi.org/10.1111/1365-2664.12607.

Seibold, Sebastian, Rammer, Werner, Hothorn, Torsten, Müller, Jörg, 2021. The contribution of insects to global forest deadwood decomposition. Nature 597, 77–81. https://doi.org/10.1038/s41586-021-03740-8.

Seidel, D., Annighöfer, P., Ehbrecht, M., Magdon, P., Wöllauer, S., Ammer, C., 2020. Deriving stand structural complexity from airborne laser scanning data—what does it tell us about a forest? Rem. Sens. 12, 1854. https://doi.org/10.3390/rs12111854.

Seidl, R., Turner, M.G., 2022. Post-disturbance reorganization of forest ecosystems in a changing world. Proc. Natl. Acad. Sci. USA 119, e2202190119. https://doi.org/10.1073/pnas.2202190119.

Senf, C., Seidl, R., 2021. Mapping the forest disturbance regimes of Europe. Nat. Sustain. 4, 63–70. https://doi.org/10.1038/s41893-020-00609-y.

Senf, C., Sebald, J., Seidl, R., 2021. Increasing canopy mortality affects the future demographic structure of Europe's forests. One Earth 4, 749–755. https://doi.org/10.1016/j.oneear.2021.04.008.

Silva, C.A., 2023. ForestGapR: Tropical Forest Canopy Gaps Analysis. documentation), E.R.P. (Reviews the, documentation), M.M. (Reviews the, documentation), D.R.A. de A. (Reviews the, documentation), E.N.B. (Reviews the, documentation), W.S.W.M.J. (Reviews the, documentation), D. de A.P. (Reviews the, documentation), A.C. (Reviews the, Valbuena, R., Jackson, T., Atkins, J., review), C.H. (Maintenance and, documentation), C.K. (Reviews the.

Silva, C.A., Valbuena, R., Pinagé, E.R., Mohan, M., 2019. ForestGapR: an R Package for Forest Gap Analysis from Canopy Height Models 10.

Small, D., 2011. Flattening gamma: radiometric terrain correction for SAR imagery. IEEE Trans. Geosci. Rem. Sens. 49, 3081–3093. https://doi.org/10.1109/TGRS.2011.2120616.

Su, X., Wang, M., Huang, Z., Fu, S., Chen, H.Y.H., 2019. Forest understorey vegetation: colonization and the availability and heterogeneity of resources. Forests 10, 944. https://doi.org/10.3390/f10110944.

Thom, D., Sommerfeld, A., Sebald, J., Hagge, J., Müller, J., Seidl, R., 2020. Effects of disturbance patterns and deadwood on the microclimate in European beech forests. Agric. For. Meteorol. 291, 108066 https://doi.org/10.1016/j.agrformet.2020.108066.

Trudel, M., Charbonneau, F., Leconte, R., 2012. Using RADARSAT-2 polarimetric and ENVISAT-ASAR dual-polarization data for estimating soil moisture over agricultural fields. Can. J. Rem. Sens. 38, 514–527. https://doi.org/10.5589/m12-043.

Tucker, C.J., 1979. Red and photographic infrared linear combinations for monitoring vegetation. Remote Sens. Environ. 8, 127–150. https://doi.org/10.1016/0034-4257(79)90013-0.

Vanhaelewyn, L., Van Der Straeten, D., De Coninck, B., Vandenbussche, F., 2020. Ultraviolet radiation from a plant perspective: the plant-microorganism context. Front. Plant Sci. 11, 597642 https://doi.org/10.3389/fpls.2020.597642.

Veloso, A., Mermoz, S., Bouvet, A., Le Toan, T., Planells, M., Dejoux, J.-F., Ceschia, E., 2017. Understanding the temporal behavior of crops using Sentinel-1 and Sentinel-2-like data for agricultural applications. Remote Sens. Environ. 199, 415–426. https://doi.org/10.1016/j.rse.2017.07.015.

Vogelmann, J.E., Rock, B.N., 1988. Assessing forest damage in high-elevation coniferous forests in Vermont and New Hampshire using thematic mapper data. Remote Sens. Environ. 24, 227–246. https://doi.org/10.1016/0034-4257(88)90027-2.

Vollrath, A., Mullissa, A., Reiche, J., 2020. Angular-based radiometric slope correction for sentinel-1 on Google earth engine. Rem. Sens. 12, 1867. https://doi.org/10.3390/rs12111867.

Webster, C., Mazzotti, G., Essery, R., Jonas, T., 2020. Enhancing airborne LiDAR data for improved forest structure representation in shortwave transmission models. Remote Sens. Environ. 249, 112017 https://doi.org/10.1016/j.rse.2020.112017.

Wood, S.N., 2017. Generalized additive models: an introduction with R. In: Chapman & Hall/CRC Texts in Statistical Science, second ed. CRC Press/Taylor & Francis Group, Boca Raton.

Zehner, M., Dubois, C., Thiel, C., Schellenberg, K., Rüetschi, M., Brenning, A., Baade, J., Schmullius, C., 2023. Accounting for deciduous forest structure and viewing geometry effects improves sentinel-1 time series image consistency. IEEE Trans. Geosci. Rem. Sens. 61, 1–13. https://doi.org/10.1109/TGRS.2023.3310113.

Zellweger, F., Baltensweiler, A., Schleppi, P., Huber, M., Küchler, M., Ginzler, C., Jonas, T., 2019. Estimating below-canopy light regimes using airborne laser scanning: an application to plant community analysis. Ecol. Evol. 9, 9149–9159. https://doi.org/10.1002/ece3.5462.

Zenner, E.K., Peck, J.E., Hobi, M.L., Commarmot, B., 2016. Validation of a classification protocol: meeting the prospect requirement and ensuring distinctiveness when assigning forest development phases. Appl. Veg. Sci. 19, 541–552. https://doi.org/10.1111/avsc.12231.